

# Upper Limit on the QCD Axion Mass from Isolated Neutron Star Cooling

Malte Buschmann,<sup>1</sup> Christopher Dessert,<sup>2,3,4</sup> Joshua W. Foster,<sup>5</sup> Andrew J. Long,<sup>6</sup> and Benjamin R. Safdi<sup>3,4</sup>

<sup>1</sup>*Department of Physics, Princeton University, Princeton, NJ 08544, U.S.A.*

<sup>2</sup>*Leinweber Center for Theoretical Physics, Department of Physics,  
University of Michigan, Ann Arbor, MI 48109 U.S.A.*

<sup>3</sup>*Berkeley Center for Theoretical Physics, University of California, Berkeley, CA 94720, U.S.A.*

<sup>4</sup>*Theoretical Physics Group, Lawrence Berkeley National Laboratory, Berkeley, CA 94720, U.S.A.*

<sup>5</sup>*Center for Theoretical Physics, Massachusetts Institute of Technology, Cambridge, Massachusetts 02139, U.S.A*

<sup>6</sup>*Department of Physics and Astronomy, Rice University, Houston, TX 77005, U.S.A.*

(Dated: November 22, 2021)

The quantum chromodynamics (QCD) axion may modify the cooling rates of neutron stars (NSs). The axions are produced within the NS cores from nucleon bremsstrahlung and, when the nucleons are in superfluid states, Cooper pair breaking and formation processes. We show that four of the nearby isolated Magnificent Seven NSs along with PSR J0659 are prime candidates for axion cooling studies because they are coeval, with ages of a few hundred thousand years known from kinematic considerations, and they have well-measured surface luminosities. We compare these data to dedicated NS cooling simulations incorporating axions, profiling over uncertainties related to the equation of state, NS masses, surface compositions, and superfluidity. Our calculations of the axion and neutrino emissivities include high-density suppression factors that also affect SN 1987A and previous NS cooling limits on axions. We find no evidence for axions in the isolated NS data, and within the context of the KSVZ QCD axion model we constrain  $m_a \lesssim 16$  meV at 95% confidence. An improved understanding of NS cooling and nucleon superfluidity could further improve these limits or lead to the discovery of the axion at weaker couplings.

The quantum chromodynamics (QCD) axion is a well-motivated beyond-the-Standard-Model particle candidate that may explain the absence of the neutron electric dipole moment [1–4] and the dark matter (DM) in our Universe [5–7]. However, the axion remains remarkably unconstrained experimentally and observationally, despite nearly 45 years of effort dedicated to axion searches (see [8] for a review). The QCD axion is primarily characterized by its decay constant  $f_a$ , which sets both its mass [9]  $m_a \approx 5.7 \mu\text{eV} (10^{12} \text{ GeV}/f_a)$  and its interaction strengths with matter. Requiring  $f_a$  below the Planck scale implies  $m_a \gtrsim 10^{-12}$  eV. The axion mass is currently bounded from above by supernova (SN) and stellar cooling constraints at the level of tens of meV, subject to model dependence and astrophysical uncertainties that are discussed further below. This work aims to improve upon these upper bounds by studying the cooling of old neutron stars (NSs) with ages  $\sim 10^5$ – $10^6$  yrs.

The NS constraints presented in this work are part of a broader effort to probe the QCD axion over its full possible mass range. Black hole superradiance disfavors QCD axion masses  $m_a < 2 \times 10^{-11}$  eV [10–12], while the ADMX experiment has reached sensitivity to Dine-Fischler-Srednicki-Zhitnitsky (DFSZ) [13, 14] QCD axion DM over the narrow mass range  $m_a \sim 2.66$ – $3.31 \mu\text{eV}$  by using the axion-photon coupling [15, 16]. Apart from these constraints, and additional narrow-band constraints from the ADMX [17] and HAYSTAC [18] experiments at the level of the more strongly-coupled Kim-Shifman-Vainshtein-Zakharov (KSVZ) [19, 20] axion, there is nearly a decade of orders of magnitude of parameter space open for the axion mass that is unprobed at present. On the other hand, near-term plans

exist to cover experimentally most of the remaining parameter space for QCD axion DM, including ABRA-CADABRA [21–23], DM-Radio [24], and CASPER [25–27] at axion masses  $m_a \ll \mu\text{eV}$ , ADMX and HAYSTAC at axion masses  $m_a \sim 1$ – $100 \mu\text{eV}$ , and MADMAX and plasma haloscopes at masses  $\sim 40$ – $400 \mu\text{eV}$  [28, 29]. However, astrophysical searches such as that presented in this work play an important role in constraining higher axion masses near and above the meV scale. Axions with  $m_a \gtrsim \text{meV}$  are difficult to probe in the laboratory, even under the non-trivial assumption that the axion is DM (but see [30, 31] for a proposal). While it was previously thought that the QCD axion cannot explain the entirety of DM at masses at and above  $\sim \text{meV}$  masses, this assumption has been challenged recently (see, *e.g.*, [32, 33]), further motivating the search for meV-scale axions.

The fundamental idea behind how axions may modify NS cooling is that these particles, just like neutrinos [34], may be produced in thermal scattering processes within the NS cores and escape the stars due to their weak interactions [35, 36]. Most previous studies of axion-induced NS cooling have focused on either proto-NSs, like that from SN 1987A [37–41], that are seconds old or young NSs like Cas A [42–48], which has an age  $\sim 300$  yrs. In this work we show that robust and competitive constraints on  $m_a$  may be found from analyses of older NS cooling, focusing on NSs with ages  $\sim 10^5$ – $10^6$  yrs. This is important when considering the possible issues that affect the SN 1987A and Cas A constraints, such as the lack of fully self-consistent 3D simulations [38] for SN 1987A and uncertainties related to the formation of the proto-NS [49]. Axion constraints from Cas A arise by using the observed temperature drop of the young NS over the

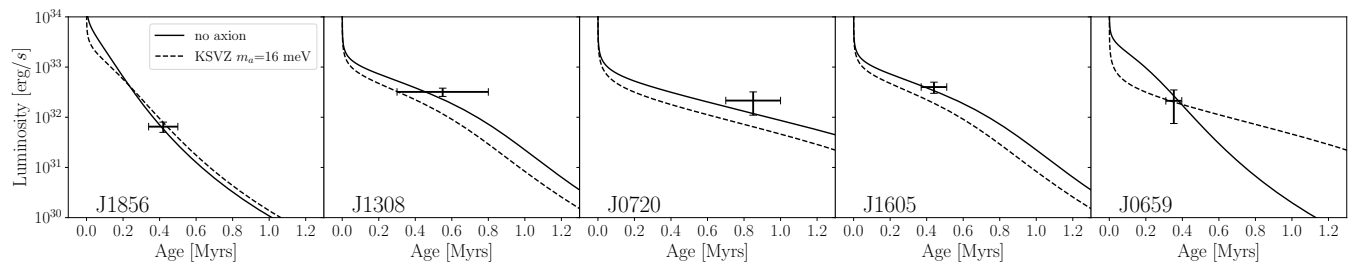


Figure 1. The luminosity and age data for each of the NSs considered in this work (see Tab. I). We show the best-fit cooling curves computed in this work for each of these NSs under the null hypothesis and with the axion mass fixed to  $m_a = 16$  meV, which is our 95% upper limit on the QCD axion mass in the context of the KSVZ model.

past  $\sim$ two decades by the *Chandra* telescope, but it was realized recently that this drop may be due in large part to a systematic evolution of the energy calibration of the detector over time [50]. Moreover, the Cas A constraints are typically derived under the assumptions of specific superfluidity and equation of state (EOS) models, which are themselves uncertain. While the importance of the SN 1987A and Cas A results should not be discounted, it is clear that additional, independent probes are needed to robustly disfavor or detect the QCD axion at masses above a few meV.

**Isolated NS data and modeling.**— In this work we use luminosity and kinematic age data from four of the seven Magnificent Seven (M7) NSs, which are those where kinematic age data is available (see Tab. I and Fig. 1 for their relevant data). We add to this list PSR J0659, identified with the Monogem Ring, as it also has an age above  $10^5$  yrs known from kinematic considerations [51, 52] and a thermal luminosity measurement. The NSs with ages  $\sim 10^5$  yrs live at a unique era, as illustrated in Fig. 2, where cooling from axion bremsstrahlung emission is maximally important; at lower ages neutrino emission plays a more important role since the neutrino (axion) emissivity scales as  $\propto T^8$  ( $T^6$ ) with temperature  $T$ , while at older ages the thermal surface emission dominates the energy loss. We discuss NSs with ages less than  $10^5$  yrs, including Cas A, in the Supplementary Material (SM). The age data have been determined by tracing the NSs back to their birthplaces. A measured NS orbit is run backwards in the Galactic potential and a parent stellar cluster is identified in each case. J1856 and J1308 are found to originate in the Upper Scorpius OB association [53, 54]. J0720 was likely born in the Trumpler association [55]. J1605 can be associated with a runaway former binary companion, which was disrupted in a supernova [56].

The thermal luminosity data for these NSs are measured from spectral fitting of NS surface models to the X-ray spectra. The strong magnetic fields create localized temperature inhomogeneities on the surfaces, so the total thermal luminosity is a more robust observable for our purposes since it is less affected by the temperature inhomogeneities than direct temperature measurements. For this reason we use the luminosity data in this work rather

than surface temperature measurements [57]. Typically, one of a NS atmosphere model or a double-blackbody model is fit to the X-ray spectral data. For J1856, a thin partially ionized hydrogen atmosphere model suggests our lower luminosity bound  $\sim 5 \times 10^{31}$  erg/s [58] while a double blackbody model suggests the upper bound  $\sim 8 \times 10^{31}$  erg/s [59]. For J1308, the same models suggest  $(3.3 \pm 0.5) \times 10^{32}$  erg/s and  $2.6 \times 10^{32}$  erg/s, respectively [60]. For J0720, both types of models give similar luminosities  $\sim 2 \times 10^{32}$  erg/s [55]. A double blackbody fit yields the luminosity  $(4 \pm 1) \times 10^{32}$  erg/s for J1605, which we adopt in our analysis [61]. The J0659 luminosity was determined with a double blackbody model including a power law, since it emits non-thermally in hard X-rays as it is a pulsar [62]. We assume Gaussian priors on the NS luminosities and ages that include all measurements at  $1\sigma$ . Note that the M7 have previously been the subject of searches for axion-induced hard X-ray emission [63, 64].

In this work we build off of the one-dimensional NS cooling code NSCool [65] to simulate NS cooling curves with axion energy losses. NSCool solves the energy balance and transport equations in full General Relativity in the core and crust of the NS. An envelope model  $T_s(T_b)$  that relates the interior and surface temperatures,  $T_b$  and  $T_s$  respectively, is glued to the exterior of the crust. After thermal relaxation, so that the NS has a uniform core temperature, integrating the energy balance equation over the interior of the NS leads to the cooling equation

$$L_\gamma^\infty = -C \frac{dT_b^\infty}{dt} - L_\nu^\infty - L_a^\infty + H, \quad (1)$$

where  $L_\gamma^\infty = 4\pi R_{*,\infty}^2 (T_s^\infty)^4$  is the photon luminosity, and  $t$  is time. (Throughout this Letter, the infinity superscript will indicate that the value is taken to be that as measured by a distant observer.) The heat capacity of the NS is  $C$ ,  $L_\nu^\infty$  is the neutrino luminosity,  $L_a^\infty$  is the axion luminosity, and  $H$  accounts for possible heating sources, such as from magnetic field decay (see Fig. 2 for an illustration). Note that we include important corrections to the neutrino emissivities relative to those in NSCool [65], which we discuss shortly, and we also assume that  $H = 0$ , since magnetic field induced heating likely plays a subdominant role in constraining  $L_a^\infty$

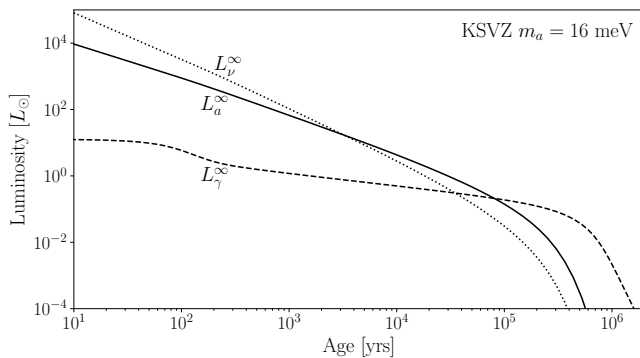


Figure 2. The luminosity production from neutrinos, axions, and surface radiation for an example NS with the KSVZ axion at  $m_a = 16$  meV. The NS parameters have been chosen to be those found in the profile likelihood procedure for J1605 with this axion mass: the BSk22 EOS, SBF-0-0 superfluidity model,  $M_{\text{NS}} = 1.0 M_{\odot}$ , and  $\Delta M/M_{\odot} = 10^{-12}$ .

(see the SM). The solution of this equation yields the NS cooling curve  $L_{\gamma}^{\infty}(t, \theta)$ , where  $\theta$  parameterizes the particular choices of axion and NS properties. The axion is parameterized by its mass  $m_a$  and coupling constants to nucleons, while for the NS we need to know (i) the NS mass  $M_{\text{NS}}$ , (ii) the equation of state (EOS), (iii) the superfluidity model  $\Delta(T_b)$ , and (iv) the envelope model parameterized by the mass of light elements  $\Delta M$ .

The axion energy losses from nucleon scattering processes are determined by the axion-neutron and axion-proton dimensionless coupling constants  $C_p$  and  $C_n$ , respectively, in addition to  $f_a$ ; the axion-nucleon interactions are of the form  $\mathcal{L} \supset (C_N/2f_a)\bar{\psi}_N\gamma^{\mu}\gamma_5\psi_N\partial_{\mu}a$  with  $N = p, n$ ,  $\psi_N$  the nucleon fields, and  $a$  the axion field. In the KSVZ axion model  $C_p = -0.47 \pm 0.03$  and  $C_n = -0.02 \pm 0.03$  [9], while in the DFSZ model  $C_p$  and  $C_n$  are functions of  $\tan\beta$ , which is the ratio of the vacuum expectation values of the up- to down-type Higgs doublets in that theory:  $C_n = (-0.160 \pm 0.025) + 0.414 \sin^2\beta$ ,  $C_p = (-0.182 \pm 0.025) - 0.435 \sin^2\beta$  [9]. Additional axion models are also possible [66], for which it is useful to define the dimensionless coupling constants  $g_{aNN} = C_N m_N / f_a$ , with  $m_N$  the nucleon mass. Note that the uncertainties on the KSVZ and DFSZ axion couplings arise from lattice QCD [9]; to make contact with previous literature we assume the central values.

When computing the axion luminosities we account for axion bremsstrahlung [35, 36] from nucleons and axion production from Cooper pair breaking and formation (PBF). If the NS core temperature is below the superfluid critical temperature, nucleons form Cooper pairs and condense into a superfluid phase. These Cooper pairs can liberate energy in the form of neutrinos [67, 68] or axions [46, 69] when breaking and forming. The PBF processes may dominate the axion luminosity at temperatures near the superfluid transition temperature, while the bremsstrahlung processes are exponentially suppressed at lower temperatures. To eval-

| Name  | $L_{\gamma}^{\infty}$ [ $10^{33}$ erg/s] | Age [Myr]        | Refs         |
|-------|--|------------------|--------------|
| J1856 | $0.065 \pm 0.015$                        | $0.42 \pm 0.08$  | [53, 58, 59] |
| J1308 | $0.32 \pm 0.06$                          | $0.55 \pm 0.25$  | [54, 60]     |
| J0720 | $0.22 \pm 0.11$                          | $0.85 \pm 0.15$  | [55, 71]     |
| J1605 | $0.4 \pm 0.1$                            | $0.44 \pm 0.07$  | [56, 61]     |
| J0659 | $0.28 \pm 0.14$                          | $0.35 \pm 0.044$ | [52, 62]     |

Table I. The properties of the NSs considered in this work – RX J1856.6–3754, RX J1308.6+2127, RX J0720.4–3125, RX J1605.3+3249, PSR J0659+1414 – which we abbreviate throughout this Letter. We include all known NSs with ages above  $10^5$  yrs and robust age and luminosity measurements (see *e.g.* [51]). Younger NSs are discussed in the SM.

uate the axion and neutrino emission rates, for both PBF and bremsstrahlung production, we account for the medium-dependent axion-nucleon and pion-nucleon couplings [70], which have not been included in earlier work on axion emission from compact stars or supernovae. These corrections are density dependent, varying throughout the interior of the star, and at the highest densities the overall effect is a  $\sim 30\%$  suppression of the axion emission rate and a  $\sim 50\%$  enhancement of the neutrino rate. See the SM for details.

We make one additional modification to NSCool to help quantify the effects of astrophysical uncertainties. The addition of light elements (hydrogen, helium, and carbon) in the NS envelope changes the expected relation between the surface and core temperatures, which in turn affects the observed surface luminosity even for the same internal state. We incorporate the analytic formulae in [72] into NSCool in order to cool a NS with a mass  $\Delta M$  of light elements layered on top of the default iron surface. Values for  $\Delta M$  can span from  $0 M_{\odot}$ , such that the NS has a pure iron surface, to  $\sim 10^{-7} M_{\odot}$ , which is the mass of the entire envelope. In practice, we modify the equation  $T_s(T_b)$  to account for the addition of light elements, which can change the photon luminosity of the NS by up to a factor  $\sim 5$  before the photon cooling stage and  $\gtrsim 100$  after. Since each  $\Delta M$  value requires a dedicated NSCool simulation, we use a discrete number eight of equally log-spaced values for  $\Delta M/M_{\odot}$  ranging from  $10^{-20} M_{\odot}$  to  $10^{-6} M_{\odot}$ . Similarly, we discretize the NS mass range with six equally spaced masses between  $1 M_{\odot}$  and  $2 M_{\odot}$ ; we show in the SM that our results are not strongly dependent on this mass range.

We simulate NSs for five distinct EOSs: APR [73], BSk22, BSk24, BSk25, and BSk26 [74]. The APR EOS is constructed using variational methods to model the two-nucleon interaction incorporating the effects of many-body interactions and with the input of nucleon-nucleon scattering data. The BSk family of EOSs are generated by fitting the Skyrme effective interaction to atomic mass data. The distinct BSk EOSs are constructed with different assumed values of the Skyrme symmetry energy. These EOSs phenomenologically characterize the range of possible stiffnesses of the EOSs. Recently, data from the NICER telescope has allowed for the simultaneous

measurements of the mass and radius of two NSs, PSR J0030 [75] and PSR J0740 [76], which can be used in conjunction with gravitational wave observations of NS mergers to constrain the EOS [76]. As we show in SM Fig. S3, only the BSk22, BSk24, and BSk25 EOS are consistent with the mass-radius data to within  $1-2\sigma$  significance. We thus restrict ourselves to this set of EOS in the main Letter, though we discuss how our results change with the APR and BSk26 EOS in the SM.

We consider three distinct superfluidity models, denoted in NSCool and here as 0-0-0, SFB-0-0, and SFB-0-T73. The first model assumes no superfluidity by setting the gaps to zero. The second model turns on the  $^1S_0$  neutron pairing gap from [77], and the third model additionally turns on the  $^1S_0$  proton pairing gap from [78]. Neutron  $^3P_2$ - $^3F_2$  pairing may also be possible (we will refer to this as  $^3P_2$  for brevity), but the estimate of this gap is more complicated in part because it appears at higher density where many-body interactions are more important (see, *e.g.*, [79]). However, in the SM we show that the  $^3P_2$  superfluid would only increase the strength of our limit, though many  $^3P_2$  gap models are inconsistent with the isolated NS data.

**Data analysis and results.**— Given the set of cooling curves, we can compare them to the observed data in Tab. I. For a given QCD axion model, under the assumption of a particular NS EOS and superfluidity model  $\Delta(T_b)$ , let us label the present-day luminosity of a NS by  $L(m_a, \theta)$ . The luminosity of NS  $i$  is then jointly determined by the axion mass  $m_a$  and the nuisance parameters  $\theta^i = \{M_{\text{NS}}^i, \Delta M^i, t^i\}$  that characterize the NS. We can now write the likelihood for a single NS  $i$  as

$$\mathcal{L}_i(\mathbf{d}_i | m_a, \theta^i) = \mathcal{N}(L(m_a, \theta^i) - L_0^i, \sigma_L^i) \times \mathcal{N}(t^i - t_0^i, \sigma_t^i), \quad (2)$$

where we have introduced the NS data set  $\mathbf{d}_i = \{L_0^i, \sigma_L^i, t_0^i, \sigma_t^i\}$ , where  $L_0^i$  is the measured luminosity of the NS with uncertainty  $\sigma_L^i$ . Similarly,  $t_0^i$  is the measured age of the NS with uncertainty  $\sigma_t^i$ . The probability of observing a value  $x$  under the zero-mean Gaussian distribution with standard deviation  $\sigma$  is denoted by  $\mathcal{N}(x, \sigma)$ . The joint likelihood  $\mathcal{L}(\mathbf{d} | m_a, \theta)$  over all five NSs is constructed by taking the product of (2) over the NSs. Note that the total list of model parameters is denoted by  $\theta = \{\theta^i\}_{i=1}^5$ . The best-fit axion mass  $\hat{m}_a$  and nuisance parameters  $\hat{\theta}$  can be determined for a given choice of EOS and superfluidity model by maximizing the joint likelihood. To test for systematic mismodeling we allow  $m_a < 0$ , with the axion luminosity multiplied by  $\text{sign}(m_a)$ .

Additionally, given the large number of nuisance parameters, many of which have non-trivial degeneracy with the signal parameter  $m_a$ , we determine the 95% upper limit on  $m_a$ , defined by  $m_a^{95}$ , by the Neyman construction of the 95% confidence interval for  $m_a$  through a Monte Carlo (MC) procedure rather than by invoking Wilks' theorem. Similarly, we determine the significance

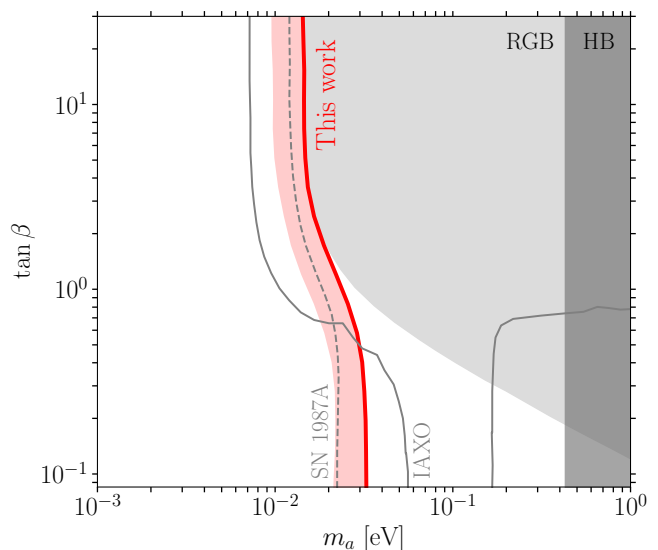


Figure 3. Upper limit from this work on the DFSZ axion mass  $m_a$  as a function of  $\tan \beta$ , which controls the relative coupling of the axion to neutrons and protons. The width of the shaded red band reflects the uncertainty on the upper limit by varying over superfluidity and EOS models. We compare our upper limits to existing constraints and the projected IAXO discovery sensitivity.

of the axion model over the null hypothesis through MC simulations of the null hypothesis, instead of relying on Wilks' theorem. (See the SM for details.)

For each combination of EOS and superfluidity model we determine  $m_a^{95}$ ,  $\hat{m}_a$ , and the significance of the axion model over the null hypothesis of  $m_a = 0$  meV. We choose the 95% upper limit over the ensemble of nine EOS and superfluidity combinations that gives the most conservative limit. For the KSVZ axion model we find that  $m_a^{95} \approx 16$  meV with the BSk22 EOS model and the SFB-0-0 superfluidity model; the strongest constraint over all combinations is  $m_a^{95} \approx 6$  meV with the BSk25 EOS and the SFB-0-T73 model. With that said, the SFB-0-T73 model is the worst fit to the data, with the best-fit axion mass being negative at  $\sim 1.6\sigma$  significance. The best-fitting model is that with the BSk22 EOS and no superfluidity, for which the limit is  $m_a^{95} \approx 14$  meV and the best-fit axion mass being negative at  $\sim 0.36\sigma$ . From these results we conclude that the NS cooling data show no evidence for the KSVZ axion and also no significant evidence for a preference for a particular EOS or superfluidity combination; the isolated NS data appear well described by the null hypothesis.

For the DFSZ axion the results depend on the value of  $\tan \beta$ . In Fig. 3 we show  $m_a^{95}$  as a function of  $\tan \beta$ , with the shaded band showing the range of limits found over all EOS and superfluidity combinations. DFSZ axion masses to the right of the exclusion curve are disfavored at 95% confidence. The weakest limit (bold) is achieved for all  $\tan \beta$  for the no superfluidity model

with the BSk22 EOS. We compare these upper limits to those from horizontal branch (HB) [80, 81], red giant branch (RGB) [82, 83], and SN 1987A [40] cooling. Note, however, that the SN 1987A limit is approximate, since e.g. it arises from the rough requirement  $L_a^1 < L^1$  for the proto-NS, and also it does not account for the density-dependent couplings for axions and neutrinos, which we estimate should weaken the SN 1987A limit by a factor 1.3{1.6, depending on the EOS. We also show the projected discovery reach for the future IAXO experiment [84]; our results leave open a narrow mass range  $\sim 10$  meV where IAXO may discover the QCD axion. In the axion model with only an axion-neutron (axion-proton) coupling we constrain  $|g_{ann}| < 1.3 \cdot 10^{-9}$  ( $|g_{app}| < 1.5 \cdot 10^{-9}$ ) at 95% confidence.

Discussion.] In this Letter we present a search for the QCD axion from NS cooling, comparing NS cooling simulations with axions to luminosity and kinematically-determined age data from  $\nu_e$  NSs. Four of the  $\nu_e$  NSs are part of the M7, which are unique in that they only emit radiation thermally and thus have well-measured thermal luminosities. The NSs that are most important for our analysis are J0720, J1605, and J1308, as further highlighted in the SM.

Our upper limits disfavor at 95% QCD axions with masses  $m_a \sim 10 - 30$  meV, depending on the axion model, which constrains the axion interpretation of the previously-observed stellar cooling anomalies [85]. The limits may be stronger if  ${}^3P_2$  superfluidity is active in the NS cores, as we discuss in the SM, though large  ${}^3P_2$  gaps appear disfavored by the isolated NS data. Many-body nuclear techniques should provide improved esti-

mates of the energy gaps of the  ${}^1S_0$  (neutron),  ${}^1S_0$  (proton), and  ${}^3P_2$  (neutron) pairings in the future [79]. On the other hand, more work should be done to rigorously assess the possible impact of heating mechanisms such as magnetic field decay on the axion limits, for example using fully self-consistent simulations along the lines of those in [86, 87]. Axions may also be produced from more exotic forms of matter in the NS interiors, such as hyperon superfluids and pionic and kaonic Bose Einstein condensates, and these channels should be investigated as the NS EOS and composition becomes better understood.

#### ACKNOWLEDGMENTS

We thank K. Cranmer, S. McDermott, T. Opferkuch, G. Raelt, and S. Witte for useful discussions and T. Opferkuch for sharing data related to the EOS. M.B. was supported by the DOE under Award Number DESC0007968. A.J.L. was supported in part by the National Science Foundation under Award No. 2114024. C.D. and B.R.S. were supported in part by the DOE Early Career Grant DESC0019225. JF was supported by a Pappalardo Fellowship. This research used resources from the Lawrence Livermore National Laboratory computational cluster provided by the IT Division at the Lawrence Berkeley National Laboratory, supported by the Director, Office of Science, and Office of Basic Energy Sciences, of the U.S. Department of Energy under Contract No. DE-AC02-05CH11231.

- 
- [1] R. D. Peccei and Helen R. Quinn, "CP Conservation in the Presence of Instantons," *Phys. Rev. Lett.* **38**, 1440{1443 (1977).
- [2] R. D. Peccei and Helen R. Quinn, "Constraints Imposed by CP Conservation in the Presence of Instantons," *Phys. Rev. D* **16**, 1791{1797 (1977).
- [3] Steven Weinberg, "A New Light Boson?" *Phys. Rev. Lett.* **40**, 223{226 (1978).
- [4] Frank Wilczek, "Problem of Strong p and t Invariance in the Presence of Instantons," *Phys. Rev. Lett.* **40**, 279{282 (1978).
- [5] John Preskill, Mark B. Wise, and Frank Wilczek, "Cosmology of the Invisible Axion," *Phys. Lett.* **120B**, 127{132 (1983).
- [6] L. F. Abbott and P. Sikivie, "A Cosmological Bound on the Invisible Axion," *Phys. Lett.* **120B**, 133{136 (1983).
- [7] Michael Dine and Willy Fischler, "The Not So Harmless Axion," *Phys. Lett.* **120B**, 137{141 (1983).
- [8] Pierre Sikivie, "Invisible Axion Search Methods," *Rev. Mod. Phys.* **93**, 015004 (2021), [arXiv:2003.02206 \[hep-ph\]](https://arxiv.org/abs/2003.02206).
- [9] Giovanni Grilli di Cortona, Edward Hardy, Javier Pardo Vega, and Giovanni Villadoro, "The QCD axion, precisely," *JHEP* **01**, 034 (2016), [arXiv:1511.02867 \[hep-ph\]](https://arxiv.org/abs/1511.02867).
- [10] Asimina Arvanitaki, Savvas Dimopoulos, Sergei Dubovsky, Nemanja Kaloper, and John March-Russell, "String Axiverse," *Phys. Rev. D* **81**, 123530 (2010), [arXiv:0905.4720 \[hep-th\]](https://arxiv.org/abs/0905.4720).
- [11] Asimina Arvanitaki and Sergei Dubovsky, "Exploring the String Axiverse with Precision Black Hole Physics," *Phys. Rev. D* **83**, 044026 (2011), [arXiv:1004.3558 \[hep-th\]](https://arxiv.org/abs/1004.3558).
- [12] Vitor Cardoso, Oscar J. C. Dias, Gavin S. Hartnett, Matthew Middleton, Paolo Pani, and Jorge E. Santos, "Constraining the mass of dark photons and axion-like particles through black-hole superradiance," *JCAP* **03**, 043 (2018), [arXiv:1801.01420 \[gr-qc\]](https://arxiv.org/abs/1801.01420).
- [13] Michael Dine, Willy Fischler, and Mark Srednicki, "A Simple Solution to the Strong CP Problem with a Harmless Axion," *Phys. Lett. B* **104**, 199{202 (1981).
- [14] A. R. Zhitnitsky, "On Possible Suppression of the Axion Hadron Interactions. (In Russian)," *Sov. J. Nucl. Phys.* **31**, 260 (1980).
- [15] N. Du et al. (ADMX), "A Search for Invisible Axion Dark Matter with the Axion Dark Matter Experiment," *Phys. Rev. Lett.* **120**, 151301 (2018), [arXiv:1804.05750 \[hep-ex\]](https://arxiv.org/abs/1804.05750).

- [16] T. Braine *et al.* (ADMX), “Extended Search for the Invisible Axion with the Axion Dark Matter Experiment,” *Phys. Rev. Lett.* **124**, 101303 (2020), [arXiv:1910.08638 \[hep-ex\]](#).
- [17] Stephen J. Asztalos *et al.* (ADMX), “Large scale microwave cavity search for dark matter axions,” *Phys. Rev. D* **64**, 092003 (2001).
- [18] K. M. Backes *et al.* (HAYSTAC), “A quantum-enhanced search for dark matter axions,” *Nature* **590**, 238–242 (2021), [arXiv:2008.01853 \[quant-ph\]](#).
- [19] Jihn E. Kim, “Weak Interaction Singlet and Strong CP Invariance,” *Phys. Rev. Lett.* **43**, 103 (1979).
- [20] Mikhail A. Shifman, A. I. Vainshtein, and Valentin I. Zakharov, “Can Confinement Ensure Natural CP Invariance of Strong Interactions?” *Nucl. Phys. B* **166**, 493–506 (1980).
- [21] Yonatan Kahn, Benjamin R. Safdi, and Jesse Thaler, “Broadband and Resonant Approaches to Axion Dark Matter Detection,” *Phys. Rev. Lett.* **117**, 141801 (2016), [arXiv:1602.01086 \[hep-ph\]](#).
- [22] Jonathan L. Ouellet *et al.*, “First Results from ABRACADABRA-10 cm: A Search for Sub- $\mu\text{eV}$  Axion Dark Matter,” *Phys. Rev. Lett.* **122**, 121802 (2019), [arXiv:1810.12257 \[hep-ex\]](#).
- [23] Chiara P. Salemi *et al.*, “Search for Low-Mass Axion Dark Matter with ABRACADABRA-10 cm,” *Phys. Rev. Lett.* **127**, 081801 (2021), [arXiv:2102.06722 \[hep-ex\]](#).
- [24] Maximiliano Silva-Feaver *et al.*, “Design Overview of DM Radio Pathfinder Experiment,” *IEEE Trans. Appl. Supercond.* **27**, 1400204 (2017), [arXiv:1610.09344 \[astro-ph.IM\]](#).
- [25] Dmitry Budker, Peter W. Graham, Micah Ledbetter, Surjeet Rajendran, and Alex Sushkov, “Proposal for a Cosmic Axion Spin Precession Experiment (CASPER),” *Phys. Rev. X* **4**, 021030 (2014), [arXiv:1306.6089 \[hep-ph\]](#).
- [26] Antoine Garcon *et al.*, “The Cosmic Axion Spin Precession Experiment (CASPER): a dark-matter search with nuclear magnetic resonance,” (2017), [10.1088/2058-9565/aa9861](#), [arXiv:1707.05312 \[physics.ins-det\]](#).
- [27] Deniz Aybas *et al.*, “Search for Axionlike Dark Matter Using Solid-State Nuclear Magnetic Resonance,” *Phys. Rev. Lett.* **126**, 141802 (2021), [arXiv:2101.01241 \[hep-ex\]](#).
- [28] P. Brun *et al.* (MADMAX), “A new experimental approach to probe QCD axion dark matter in the mass range above  $40 \mu\text{eV}$ ,” *Eur. Phys. J. C* **79**, 186 (2019), [arXiv:1901.07401 \[physics.ins-det\]](#).
- [29] Matthew Lawson, Alexander J. Millar, Matteo Pancaldi, Edoardo Vitagliano, and Frank Wilczek, “Tunable axion plasma haloscopes,” *Phys. Rev. Lett.* **123**, 141802 (2019), [arXiv:1904.11872 \[hep-ph\]](#).
- [30] Asimina Arvanitaki and Andrew A. Geraci, “Resonantly Detecting Axion-Mediated Forces with Nuclear Magnetic Resonance,” *Phys. Rev. Lett.* **113**, 161801 (2014), [arXiv:1403.1290 \[hep-ph\]](#).
- [31] A. A. Geraci *et al.* (ARIADNE), “Progress on the ARIADNE axion experiment,” *Springer Proc. Phys.* **211**, 151–161 (2018), [arXiv:1710.05413 \[astro-ph.IM\]](#).
- [32] Raymond T. Co, Lawrence J. Hall, Keisuke Harigaya, Keith A. Olive, and Sarunas Verner, “Axion Kinetic Misalignment and Parametric Resonance from Inflation,” *JCAP* **08**, 036 (2020), [arXiv:2004.00629 \[hep-ph\]](#).
- [33] Marco Gorghetto, Edward Hardy, and Giovanni Villadoro, “More Axions from Strings,” *SciPost Phys.* **10**, 050 (2021), [arXiv:2007.04990 \[hep-ph\]](#).
- [34] D. G. Yakovlev, A. D. Kaminker, Oleg Y. Gnedin, and P. Haensel, “Neutrino emission from neutron stars,” *Phys. Rept.* **354**, 1 (2001), [arXiv:astro-ph/0012122](#).
- [35] N. Iwamoto, “Axion Emission from Neutron Stars,” *Phys. Rev. Lett.* **53**, 1198–1201 (1984).
- [36] Naoki Iwamoto, “Nucleon-nucleon bremsstrahlung of axions and pseudoscalar particles from neutron star matter,” *Phys. Rev. D* **64**, 043002 (2001).
- [37] Georg G. Raffelt, “Astrophysical axion bounds,” *Lect. Notes Phys.* **741**, 51–71 (2008), [arXiv:hep-ph/0611350](#).
- [38] Tobias Fischer, Sovan Chakraborty, Maurizio Giannotti, Alessandro Mirizzi, Alexandre Payez, and Andreas Ringwald, “Probing axions with the neutrino signal from the next galactic supernova,” *Phys. Rev. D* **94**, 085012 (2016), [arXiv:1605.08780 \[astro-ph.HE\]](#).
- [39] Jae Hyeok Chang, Rouven Essig, and Samuel D. McDermott, “Supernova 1987A Constraints on Sub-GeV Dark Sectors, Millicharged Particles, the QCD Axion, and an Axion-like Particle,” *JHEP* **09**, 051 (2018), [arXiv:1803.00993 \[hep-ph\]](#).
- [40] Pierluca Carenza, Tobias Fischer, Maurizio Giannotti, Gang Guo, Gabriel Martínez-Pinedo, and Alessandro Mirizzi, “Improved axion emissivity from a supernova via nucleon-nucleon bremsstrahlung,” *JCAP* **10**, 016 (2019), [Erratum: *JCAP* **05**, E01 (2020)], [arXiv:1906.11844 \[hep-ph\]](#).
- [41] Pierluca Carenza, Bryce Fore, Maurizio Giannotti, Alessandro Mirizzi, and Sanjay Reddy, “Enhanced Supernova Axion Emission and its Implications,” *Phys. Rev. Lett.* **126**, 071102 (2021), [arXiv:2010.02943 \[hep-ph\]](#).
- [42] Dany Page, Madappa Prakash, James M. Lattimer, and Andrew W. Steiner, “Rapid Cooling of the Neutron Star in Cassiopeia A Triggered by Neutron Superfluidity in Dense Matter,” *Phys. Rev. Lett.* **106**, 081101 (2011), [arXiv:1011.6142 \[astro-ph.HE\]](#).
- [43] Peter S. Shternin, Dmitry G. Yakovlev, Craig O. Heinke, Wynn C. G. Ho, and Daniel J. Patnaude, “Cooling neutron star in the Cassiopeia A supernova remnant: evidence for superfluidity in the core,” *MNRAS* **412**, L108–L112 (2011), [arXiv:1012.0045 \[astro-ph.SR\]](#).
- [44] Lev B. Leinson, “Superfluid phases of triplet pairing and rapid cooling of the neutron star in Cassiopeia A,” *Phys. Lett. B* **741**, 87–91 (2015), [arXiv:1411.6833 \[astro-ph.SR\]](#).
- [45] L. B. Leinson, “Axion mass limit from observations of the neutron star in Cassiopeia A,” *JCAP* **08**, 031 (2014), [arXiv:1405.6873 \[hep-ph\]](#).
- [46] Armen Sedrakian, “Axion cooling of neutron stars,” *Phys. Rev.* **D93**, 065044 (2016), [arXiv:1512.07828 \[astro-ph.HE\]](#).
- [47] Koichi Hamaguchi, Natsumi Nagata, Keisuke Yanagi, and Jiaming Zheng, “Limit on the Axion Decay Constant from the Cooling Neutron Star in Cassiopeia A,” *Phys. Rev. D* **98**, 103015 (2018), [arXiv:1806.07151 \[hep-ph\]](#).
- [48] Lev B. Leinson, “Impact of axions on the Cassiopeia A neutron star cooling,” (2021), [arXiv:2105.14745 \[hep-ph\]](#).
- [49] Nitsan Bar, Kfir Blum, and Guido D’Amico, “Is there a supernova bound on axions?” *Phys. Rev. D* **101**, 123025

- (2020), [arXiv:1907.05020 \[hep-ph\]](#).
- [50] B. Posselt and G. G. Pavlov, “Upper limits on the rapid cooling of the Central Compact Object in Cas A,” *Astrophys. J.* **864**, 135 (2018), [arXiv:1808.00531 \[astro-ph.HE\]](#).
- [51] A.Y. Potekhin, D.A. Zyuzin, D.G. Yakovlev, M.V. Beznogov, and Yu.A. Shibano, “Thermal luminosities of cooling neutron stars,” *Mon. Not. Roy. Astron. Soc.* **496**, 5052–5071 (2020), [arXiv:2006.15004 \[astro-ph.HE\]](#).
- [52] Hiromasa Suzuki, Aya Bamba, and Shinpei Shibata, “Quantitative Age Estimation of Supernova Remnants and Associated Pulsars,” *Astrophys. J.* **914**, 103 (2021), [arXiv:2104.10052 \[astro-ph.HE\]](#).
- [53] R. P. Mignani, D. Vande Putte, M. Cropper, R. Turolla, S. Zane, L. J. Pellizza, L. A. Bignone, N. Sartore, and A. Treves, “The birthplace and age of the isolated neutron star RX J1856.5-3754,” *Monthly Notices of the RAS* **429**, 3517–3521 (2013), [arXiv:1212.3141 \[astro-ph.HE\]](#).
- [54] C. Motch, A. M. Pires, F. Haberl, A. Schwope, and V. E. Zavlin, “Proper motions of thermally emitting isolated neutron stars measured with Chandra,” *A&A* **497**, 423–435 (2009), [arXiv:0901.1006 \[astro-ph.HE\]](#).
- [55] N. Tetzlaff, T. Eisenbeiss, R. Neuhäuser, and M. M. Hohle, “The origin of RX J1856.5-3754 and RX J0720.4-3125 - updated using new parallax measurements,” *Monthly Notices of the RAS* **417**, 617–626 (2011), [arXiv:1107.1673 \[astro-ph.GA\]](#).
- [56] N. Tetzlaff, J. G. Schmidt, M. M. Hohle, and R. Neuhäuser, “Neutron Stars From Young Nearby Associations: The Origin of RX J1605.3+3249,” *Publications of the Astron. Soc. of Australia* **29**, 98–108 (2012), [arXiv:1202.1388 \[astro-ph.GA\]](#).
- [57] M. V. Beznogov, A. Y. Potekhin, and D. G. Yakovlev, “Heat blanketing envelopes of neutron stars,” *Phys. Rept.* **919**, 1–68 (2021), [arXiv:2103.12422 \[astro-ph.SR\]](#).
- [58] Wynn C.G. Ho, David L. Kaplan, Philip Chang, Matthew van Adelsberg, and Alexander Y. Potekhin, “Magnetic Hydrogen Atmosphere Models and the Neutron Star RX J1856.5-3754,” *Mon. Not. Roy. Astron. Soc.* **375**, 821–830 (2007), [arXiv:astro-ph/0612145](#).
- [59] N. Sartore, A. Tiengo, S. Mereghetti, A. De Luca, R. Turolla, and F. Haberl, “Spectral monitoring of RX J1856.5-3754 with XMM-Newton. Analysis of EPIC-pn data,” *Astronomy and Astrophysics* **541**, A66 (2012), [arXiv:1202.2121 \[astro-ph.HE\]](#).
- [60] V. Hambaryan, V. Suleimanov, A. D. Schwope, R. Neuhäuser, K. Werner, and A. Y. Potekhin, “Phase-resolved spectroscopic study of the isolated neutron star RBS 1223 (1RXS J130848.6+212708),” *Astronomy and Astrophysics* **534**, A74 (2011).
- [61] A.M. Pires, A.D. Schwope, F. Haberl, V.E. Zavlin, C. Motch, and S. Zane, “A deep XMM-Newton look on the thermally emitting isolated neutron star RX J1605.3+3249,” *Astron. Astrophys.* **623**, A73 (2019), [arXiv:1901.08533 \[astro-ph.HE\]](#).
- [62] S. Zharikov, D. Zyuzin, Yu. Shibano, A. Kirichenko, R. E. Mennickent, S. Geier, and A. Cabrera-Lavers, “PSR B0656+14: the unified outlook from the infrared to X-rays,” *Mon. Not. Roy. Astron. Soc.* **502**, 2005–2022 (2021), [arXiv:2101.07459 \[astro-ph.HE\]](#).
- [63] Christopher Dessert, Joshua W. Foster, and Benjamin R. Safdi, “Hard X-ray Excess from the Magnificent Seven Neutron Stars,” *Astrophys. J.* **904**, 42 (2020), [arXiv:1910.02956 \[astro-ph.HE\]](#).
- [64] Malte Buschmann, Raymond T. Co, Christopher Dessert, and Benjamin R. Safdi, “Axion Emission Can Explain a New Hard X-Ray Excess from Nearby Isolated Neutron Stars,” *Phys. Rev. Lett.* **126**, 021102 (2021), [arXiv:1910.04164 \[hep-ph\]](#).
- [65] Dany Page, “NSCool: Neutron star cooling code,” (2016), [ascl:1609.009](#).
- [66] Luca Di Luzio, Maurizio Giannotti, Enrico Nardi, and Luca Visinelli, “The landscape of QCD axion models,” *Phys. Rept.* **870**, 1–117 (2020), [arXiv:2003.01100 \[hep-ph\]](#).
- [67] E. Flowers, M. Ruderman, and P. Sutherland, “Neutrino pair emission from finite-temperature neutron superfluid and the cooling of young neutron stars.” *The Astrophysical Journal* **205**, 541–544 (1976).
- [68] A. V. Senatorov and D. N. Voskresensky, “Collective excitations in nucleonic matter and the problem of cooling of neutron stars,” *Physics Letters B* **184**, 119–124 (1987).
- [69] Jochen Keller and Armen Sedrakian, “Axions from cooling compact stars,” *Nucl. Phys.* **A897**, 62–69 (2013), [arXiv:1205.6940 \[astro-ph.CO\]](#).
- [70] Tobias Fischer, “The role of medium modifications for neutrino-pair processes from nucleon-nucleon bremsstrahlung - Impact on the proton-neutron star deleptonization,” *Astron. Astrophys.* **593**, A103 (2016), [arXiv:1608.05004 \[astro-ph.HE\]](#).
- [71] V. Hambaryan, V. Suleimanov, F. Haberl, A. D. Schwope, R. Neuhäuser, M. Hohle, and K. Werner, “The compactness of the isolated neutron star RX J0720.4-3125,” *Astron. Astrophys.* **601**, A108 (2017), [arXiv:1702.07635 \[astro-ph.HE\]](#).
- [72] A. Y. Potekhin, G. Chabrier, and D. G. Yakovlev, “Internal temperatures and cooling of neutron stars with accreted envelopes,” *Astron. Astrophys.* **323**, 415 (1997), [arXiv:astro-ph/9706148](#).
- [73] A. Akmal, V. R. Pandharipande, and D. G. Ravenhall, “Equation of state of nucleon matter and neutron star structure,” *Phys. Rev. C* **58**, 1804–1828 (1998).
- [74] J. M. Pearson, N. Chamel, A. Y. Potekhin, A. F. Fantina, C. Ducoin, A. K. Dutta, and S. Goriely, “Unified equations of state for cold non-accreting neutron stars with Brussels–Montreal functionals – I. Role of symmetry energy,” *Mon. Not. Roy. Astron. Soc.* **481**, 2994–3026 (2018), [Erratum: *Mon. Not. Roy. Astron. Soc.* **486**, 768 (2019)], [arXiv:1903.04981 \[astro-ph.HE\]](#).
- [75] Thomas E. Riley *et al.*, “A *NICER* View of PSR J0030+0451: Millisecond Pulsar Parameter Estimation,” *Astrophys. J. Lett.* **887**, L21 (2019), [arXiv:1912.05702 \[astro-ph.HE\]](#).
- [76] M. C. Miller *et al.*, “The Radius of PSR J0740+6620 from *NICER* and XMM-Newton Data,” *Astrophys. J. Lett.* **918**, L28 (2021), [arXiv:2105.06979 \[astro-ph.HE\]](#).
- [77] Achim Schwenk, Bengt Friman, and Gerald E. Brown, “Renormalization group approach to neutron matter: Quasiparticle interactions, superfluid gaps and the equation of state,” *Nucl. Phys. A* **713**, 191–216 (2003), [arXiv:nucl-th/0207004](#).
- [78] M. Baldo, J. Cugnon, A. Lejeune, and U. Lombardo, “Proton and neutron superfluidity in neutron star matter,” *Nuclear Physics A* **536**, 349–365 (1992).
- [79] Armen Sedrakian and John W. Clark, “Superfluidity in

- nuclear systems and neutron stars,” *Eur. Phys. J. A* **55**, 167 (2019), [arXiv:1802.00017 \[nucl-th\]](#).
- [80] Adrian Ayala, Inma Domínguez, Maurizio Giannotti, Alessandro Mirizzi, and Oscar Straniero, “Revisiting the bound on axion-photon coupling from Globular Clusters,” *Phys. Rev. Lett.* **113**, 191302 (2014), [arXiv:1406.6053 \[astro-ph.SR\]](#).
- [81] Oscar Straniero, Adrian Ayala, Maurizio Giannotti, Alessandro Mirizzi, and Inma Domínguez, “Axion-Photon Coupling: Astrophysical Constraints,” in *11th Patras Workshop on Axions, WIMPs and WISPs* (2015) pp. 77–81.
- [82] Nicolás Viaux, Márcio Catelan, Peter B. Stetson, Georg Raffelt, Javier Redondo, Aldo A. R. Valcarce, and Achim Weiss, “Neutrino and axion bounds from the globular cluster M5 (NGC 5904),” *Phys. Rev. Lett.* **111**, 231301 (2013), [arXiv:1311.1669 \[astro-ph.SR\]](#).
- [83] Oscar Straniero, Inmaculata Domínguez, Maurizio Giannotti, and Alessandro Mirizzi, “Axion-electron coupling from the RGB tip of Globular Clusters,” *arXiv e-prints*, [arXiv:1802.10357](#) (2018), [arXiv:1802.10357 \[astro-ph.SR\]](#).
- [84] E. Armengaud *et al.* (IAXO), “Physics potential of the International Axion Observatory (IAXO),” *JCAP* **06**, 047 (2019), [arXiv:1904.09155 \[hep-ph\]](#).
- [85] Maurizio Giannotti, Igor G. Irastorza, Javier Redondo, Andreas Ringwald, and Ken’ichi Saikawa, “Stellar Recipes for Axion Hunters,” *JCAP* **10**, 010 (2017), [arXiv:1708.02111 \[hep-ph\]](#).
- [86] Deborah N. Aguilera, Jose A. Pons, and Juan A. Miralles, “2D Cooling of Magnetized Neutron Stars,” *Astron. Astrophys.* **486**, 255–271 (2008), [arXiv:0710.0854 \[astro-ph\]](#).
- [87] A. Y. Potekhin and G. Chabrier, “Magnetic neutron star cooling and microphysics,” *Astron. Astrophys.* **609**, A74 (2018), [arXiv:1711.07662 \[astro-ph.HE\]](#).
- [88] B. L. Friman and O. V. Maxwell, “Neutron Star Neutrino Emissivities,” *Astrophys. J.* **232**, 541–557 (1979).
- [89] D. G. Yakovlev and K. P. Levenfish, “Modified URCA process in neutron star cores.” *Astronomy and Astrophysics* **297**, 717 (1995).
- [90] Ron Mayle, James R. Wilson, John R. Ellis, Keith A. Olive, David N. Schramm, and Gary Steigman, “Updated Constraints on Axions from SN 1987a,” *Phys. Lett. B* **219**, 515 (1989).
- [91] K. P. Levenfish and D. G. Yakovlev, “Suppression of neutrino energy losses in reactions of direct urca processes by superfluidity in neutron star nuclei,” *Astronomy Letters* **20**, 43–51 (1994).
- [92] D. G. Yakovlev, A. D. Kaminker, and K. P. Levenfish, “Neutrino emission due to Cooper pairing of nucleons in cooling neutron stars,” *Astron. Astrophys.* **343**, 650 (1999), [arXiv:astro-ph/9812366](#).
- [93] Brynmor Haskell and Armen Sedrakian, “Superfluidity and Superconductivity in Neutron Stars,” *Astrophys. Space Sci. Libr.* **457**, 401–454 (2018), [arXiv:1709.10340 \[astro-ph.HE\]](#).
- [94] K. P. Levenfish and D. G. Yakovlev, “Specific heat of neutron star cores with superfluid nucleons,” *Astronomy Reports* **38**, 247–251 (1994).
- [95] Dany Page, James M. Lattimer, Madappa Prakash, and Andrew W. Steiner, “Minimal cooling of neutron stars: A New paradigm,” *Astrophys. J. Suppl.* **155**, 623–650 (2004), [arXiv:astro-ph/0403657](#).
- [96] K. P. Levenfish and D. G. Yakovlev, “Standard and enhanced cooling of neutron stars with superfluid cores,” *Astron. Lett.* **22**, 49 (1996), [arXiv:astro-ph/9608032](#).
- [97] Dany Page, James M. Lattimer, Madappa Prakash, and Andrew W. Steiner, “Neutrino Emission from Cooper Pairs and Minimal Cooling of Neutron Stars,” *Astrophys. J.* **707**, 1131–1140 (2009), [arXiv:0906.1621 \[astro-ph.SR\]](#).
- [98] Glen Cowan, Kyle Cranmer, Eilam Gross, and Ofer Vitells, “Asymptotic formulae for likelihood-based tests of new physics,” *Eur. Phys. J. C* **71**, 1554 (2011), [Erratum: *Eur.Phys.J.C* 73, 2501 (2013)], [arXiv:1007.1727 \[physics.data-an\]](#).
- [99] Jr. Ashworth, W. B., “A Probable Flamsteed Observation of the Cassiopeia A Supernova,” *Journal for the History of Astronomy* **11**, 1 (1980).
- [100] Robert A. Fesen, Molly C. Hammell, Jon Morse, Roger A. Chevalier, Kazimierz J. Borkowski, Michael A. Dopita, Christopher L. Gerardy, Stephen S. Lawrence, John C. Raymond, and Sidney van den Bergh, “The expansion asymmetry and age of the cassiopeia a supernova remnant,” *Astrophys. J.* **645**, 283–292 (2006), [arXiv:astro-ph/0603371](#).
- [101] D. Klochkov, V. Suleimanov, G. Pühlhofer, D. G. Yakovlev, A. Santangelo, and K. Werner, “The neutron star in HESSJ1731-347: Central compact objects as laboratories to study the equation of state of superdense matter,” *Astron. Astrophys.* **573**, A53 (2015), [arXiv:1410.1055 \[astro-ph.HE\]](#).
- [102] F. Acero, M. Lemoine-Goumard, M. Renaud, J. Ballet, J. W. Hewitt, R. Rousseau, and T. Tanaka, “Study of TeV shell supernova remnants at gamma-ray energies,” *Astron. Astrophys.* **580**, A74 (2015), [arXiv:1506.02307 \[astro-ph.HE\]](#).
- [103] Y. Cui, G. Pühlhofer, and A. Santangelo, “A young supernova remnant illuminating nearby molecular clouds with cosmic rays,” *Astron. Astrophys.* **591**, A68 (2016), [arXiv:1605.00483 \[astro-ph.HE\]](#).
- [104] Nigel Maxted, Michael Burton, Catherine Braiding, Gavin Rowell, Hidetoshi Sano, Fabien Voisin, Massimo Capasso, Gerd Pühlhofer, and Yasuo Fukui, “Probing the local environment of the supernova remnant HESS J1731–347 with CO and CS observations,” *Mon. Not. Roy. Astron. Soc.* **474**, 662–676 (2018), [arXiv:1710.06101 \[astro-ph.HE\]](#).
- [105] Wynn C. G. Ho, Yue Zhao, Craig O. Heinke, D. L. Kaplan, Peter S. Shternin, and M. J. P. Wijngaarden, “X-ray bounds on cooling, composition, and magnetic field of the Cassiopeia A neutron star and young central compact objects,” *Mon. Not. Roy. Astron. Soc.* **506**, 5015–5029 (2021), [arXiv:2107.08060 \[astro-ph.HE\]](#).
- [106] I. Lovchinsky, P. Slane, B. M. Gaensler, J. P. Hughes, C. Y. Ng, J. S. Lazendic, J. D. Gelfand, and C. L. Brogan, “A Chandra Observation of Supernova Remnant G350.1-0.3 and Its Central Compact Object,” *The Astrophysical Journal* **731**, 70 (2011), [arXiv:1102.5333 \[astro-ph.HE\]](#).
- [107] Martin G. F. Mayer and Werner Becker, “A kinematic study of central compact objects and their host supernova remnants,” *Astron. Astrophys.* **651**, A40 (2021), [arXiv:2106.00700 \[astro-ph.HE\]](#).
- [108] Aida Kirichenko, Andrey Danilenko, Yury Shibanov, Peter Shternin, Sergey Zharikov, and Dmitry Zyuzin, “Deep optical observations of the  $\gamma$ -ray pul-

- sar J0357+3205,” *Astron. Astrophys.* **564**, A81 (2014), [arXiv:1402.2246 \[astro-ph.SR\]](#).
- [109] Chi-Y. Ng, Roger W. Romani, Walter F. Brisken, Shami Chatterjee, and Michael Kramer, “The Origin and Motion of PSR J0538+2817 in S147,” *Astrophys. J.* **654**, 487–493 (2006), [arXiv:astro-ph/0611068](#).
- [110] Craig O. Heinke and Wynn C. G. Ho, “Direct Observation of the Cooling of the Cassiopeia A Neutron Star,” *The Astrophysical Journal, Letters* **719**, L167–L171 (2010), [arXiv:1007.4719 \[astro-ph.HE\]](#).
- [111] K.G. Elshamouty, C.O. Heinke, G.R. Sivakoff, W.C.G. Ho, P.S. Shternin, D.G. Yakovlev, D.J. Patnaude, and L. David, “Measuring the Cooling of the Neutron Star in Cassiopeia A with all Chandra X-ray Observatory Detectors,” *Astrophys. J.* **777**, 22 (2013), [arXiv:1306.3387 \[astro-ph.HE\]](#).
- [112] Mikhail V. Beznogov, Ermal Rrapaj, Dany Page, and Sanjay Reddy, “Constraints on Axion-like Particles and Nucleon Pairing in Dense Matter from the Hot Neutron Star in HESS J1731-347,” *Phys. Rev. C* **98**, 035802 (2018), [arXiv:1806.07991 \[astro-ph.HE\]](#).
- [113] Lev B. Leinson, “Constraints on axions from neutron star in HESS J1731-347,” *JCAP* **11**, 031 (2019), [arXiv:1909.03941 \[hep-ph\]](#).
- [114] W. W. Tian, D. A. Leahy, M. Haverkorn, and B. Jiang, “Discovery of the counterpart of TeV Gamma-ray source HESS J1731-347: a new SNR G353.6-0.7 with radio and X-ray images,” *Astrophys. J. Lett.* **679**, L85 (2008), [arXiv:0801.3254 \[astro-ph\]](#).
- [115] D. Ding, A. Rios, H. Dussan, W. H. Dickhoff, S. J. Witte, A. Polls, and A. Carbone, “Pairing in high-density neutron matter including short- and long-range correlations,” *Phys. Rev. C* **94**, 025802 (2016), [Addendum: *Phys.Rev.C* 94, 029901 (2016)], [arXiv:1601.01600 \[nucl-th\]](#).
- [116] Shao-Peng Tang, Jin-Liang Jiang, Wei-Hong Gao, Yi-Zhong Fan, and Da-Ming Wei, “The Masses of Isolated Neutron Stars Inferred from the Gravitational Redshift Measurements,” *Astrophys. J.* **888**, 45 (2020), [arXiv:1911.08107 \[astro-ph.HE\]](#).
- [117] P. Haensel, V. A. Urpin, and D. G. Yakovlev, “Ohmic decay of internal magnetic fields in neutron stars,” *Astronomy and Astrophysics* **229**, 133–137 (1990).
- [118] Juan A. Miralles, Vadim Urpin, and Denis Konenkov, “Joule heating and the thermal evolution of old neutron stars,” *Astrophys. J.* **503**, 368 (1998), [arXiv:astro-ph/9803063](#).
- [119] D. Page, U. Geppert, and T. Zannias, “General relativistic treatment of the thermal, magnetic and rotational evolution of neutron stars with crustal magnetic fields,” *Astron. Astrophys.* **360**, 1052 (2000), [arXiv:astro-ph/0005301](#).
- [120] U. Geppert, M. Rheinhardt, and J. Gil, “Spot-like structures of neutron star surface magnetic fields,” *Astron. Astrophys.* **412**, L33–L36 (2003), [arXiv:astro-ph/0311121](#).
- [121] P. Arras, A. Cumming, and Christopher Thompson, “Magnetars: Time evolution, superfluid properties, and mechanism of magnetic field decay,” *Astrophys. J. Lett.* **608**, L49–L52 (2004), [arXiv:astro-ph/0401561](#).
- [122] Andrew Cumming, Phil Arras, and Ellen G. Zweibel, “Magnetic field evolution in neutron star crusts due to the Hall effect and Ohmic decay,” *Astrophys. J.* **609**, 999–1017 (2004), [arXiv:astro-ph/0402392](#).
- [123] Jose A. Pons, Bennett Link, Juan A. Miralles, and Ulrich Geppert, “Evidence for Heating of Neutron Stars by Magnetic Field Decay,” *Phys. Rev. Lett.* **98**, 071101 (2007), [arXiv:astro-ph/0607583](#).
- [124] Jose A. Pons and U. Geppert, “Magnetic field dissipation in neutron star crusts: From magnetars to isolated neutron stars,” *Astron. Astrophys.* **470**, 303 (2007), [arXiv:astro-ph/0703267](#).
- [125] Deborah N. Aguilera, Jose A. Pons, and Juan A. Miralles, “The impact of magnetic field on the thermal evolution of neutron stars,” *Astrophys. J. Lett.* **673**, L167–L170 (2008), [arXiv:0712.1353 \[astro-ph\]](#).
- [126] S. B. Popov, J. A. Pons, J. A. Miralles, P. A. Boldin, and B. Posselt, “Population synthesis studies of isolated neutron stars with magnetic field decay,” *Mon. Not. Roy. Astron. Soc.* **401**, 2675–2686 (2010), [arXiv:0910.2190 \[astro-ph.HE\]](#).
- [127] Daniele Viganò, Nanda Rea, Jose A. Pons, Rosalba Perna, Deborah N. Aguilera, and Juan A. Miralles, “Unifying the observational diversity of isolated neutron stars via magneto-thermal evolution models,” *Mon. Not. Roy. Astron. Soc.* **434**, 123 (2013), [arXiv:1306.2156 \[astro-ph.SR\]](#).
- [128] Daniele Viganò, Alberto García-García, José A. Pons, Clara Dehman, and Vanessa Graber, “Magneto-thermal evolution of neutron stars with coupled Ohmic, Hall and ambipolar effects via accurate finite-volume simulations,” *Comput. Phys. Commun.* **265**, 108001 (2021), [arXiv:2104.08001 \[astro-ph.HE\]](#).

# Supplementary Material for Upper Limit on the QCD Axion Mass from Isolated Neutron Star Cooling

Malte Buschmann, Christopher Dessert, Joshua W. Foster, Andrew J. Long, and Benjamin R. Safdi

This Supplementary Material (SM) is organized as follows. In Sec. I we present our calculations of the axion and neutrino emissivities. Sec. II presents our statistical methodology. Sec. III gives extended results for the analyses mentioned in the main body, while Sec. IV presents our estimates for the effects of magnetic field decay on the axion upper limits.

## I. AXION AND NEUTRINO EMISSIVITIES

In this section we present the axion and neutrino emissivities that we use in the simulations discussed in the main Letter. We include a number of factors relevant for axion and neutrino production in dense media that have not previously been included in NS cooling simulations.

### A. Axion production rates

Our analysis accounts for the two dominant channels by which axions are produced in the core of a cooling NS. When the core temperature  $T$  exceeds the critical temperature  $T_c$  for the superfluid phase transition, axion emission is dominated by nucleon-nucleon bremsstrahlung. When  $T$  falls below  $T_c$ , axion emission is dominated by the formation and breaking of Cooper pairs (PBF processes). To calculate the axion production rate, we sum these two contributions.

Axion emission via nucleon-nucleon bremsstrahlung corresponds to three scattering channels:  $nn \rightarrow nna$ ,  $pp \rightarrow ppa$ , and  $np \rightarrow npa$ . For the temperatures of interest, the nucleons are strongly degenerate and non-relativistic. Expressions for the axion emissivity  $\varepsilon_a$  (energy emitted per volume per time) are provided by Refs. [35, 36]. These early derivations of the axion emissivity did not take into account various medium effects, which were pointed out in later literature, and which we have incorporated into the calculation. The axion emissivities that we use in our work are as follows:

$$nn \rightarrow nna : \quad \varepsilon_a \simeq (7.373 \times 10^{11} \text{ erg/cm}^3/\text{sec}) \left( \frac{g_{ann}}{10^{-10}} \right)^2 \left( \frac{F(x_n)}{0.601566} \right) \left( \frac{p_{F,n}}{1.68 \text{ fm}^{-1}} \right) \left( \frac{T}{10^8 \text{ K}} \right)^6 \quad (\text{S1})$$

$$\times \left( \frac{\beta_{nn}}{0.56} \right) \left( \frac{\gamma_{nn}}{0.838} \right) \left( \frac{\gamma}{1} \right)^6 \left( \frac{\mathcal{R}_{nn}}{1} \right)$$

$$pp \rightarrow ppa : \quad \varepsilon_a \simeq (9.191 \times 10^{11} \text{ erg/cm}^3/\text{sec}) \left( \frac{g_{app}}{10^{-10}} \right)^2 \left( \frac{F(x_p)}{0.601556} \right) \left( \frac{p_{F,p}}{1.68 \text{ fm}^{-1}} \right) \left( \frac{T}{10^8 \text{ K}} \right)^6 \quad (\text{S2})$$

$$\times \left( \frac{\beta_{pp}}{0.7} \right) \left( \frac{\gamma_{pp}}{0.838} \right) \left( \frac{\gamma}{1} \right)^6 \left( \frac{\mathcal{R}_{pp}}{1} \right)$$

$$np \rightarrow npa : \quad \varepsilon_a \simeq (9.617 \times 10^{11} \text{ erg/cm}^3/\text{sec}) \left( \frac{g_{\text{eff}}}{10^{-10}} \right)^2 \left( \frac{p_{F,p}}{1.68 \text{ fm}^{-1}} \right) \left( \frac{T}{10^8 \text{ K}} \right)^6 \quad (\text{S3})$$

$$\times \left( \frac{\beta_{np}}{0.66} \right) \left( \frac{\gamma_{np}}{0.838} \right) \left( \frac{\gamma}{1} \right)^6 \left( \frac{\mathcal{R}_{np}}{1} \right).$$

Note that  $1.68 \text{ fm}^{-1} \simeq 331.5 \text{ MeV}$ ,  $10^8 \text{ K} \simeq 8.617 \text{ keV}$ ,  $m_n \simeq 939.565 \text{ MeV}$ , and  $m_p \simeq 938.272 \text{ MeV}$ .

Let us now discuss each of the factors appearing in the emissivities above.

- The axion emissivity is proportional to  $g_{ann}^2$  ( $g_{app}^2$ ) if the axion couples to a neutron (proton) only. If the axion couples to both nucleons, then the axion emissivity for the process  $np \rightarrow npa$  depends on an effective

coupling [36]

$$\begin{aligned}
g_{\text{eff}} &= \sqrt{(g_{app} + g_{ann})^2 C_g + (g_{app} - g_{ann})^2 C_h} \\
C_g &= \frac{1}{2} F(x_p) + F\left(\frac{2x_n x_p}{x_n + x_p}\right) + F\left(\frac{2x_n x_p}{x_p - x_n}\right) + \frac{x_p}{x_n} F\left(\frac{2x_n x_p}{x_n + x_p}\right) - \frac{x_p}{x_n} F\left(\frac{2x_n x_p}{x_p - x_n}\right) + G(x_p) \\
C_h &= \frac{1}{2} F(x_p) + \frac{1}{2} F\left(\frac{2x_n x_p}{x_n + x_p}\right) + \frac{1}{2} F\left(\frac{2x_n x_p}{x_p - x_n}\right) + \frac{1}{2} \frac{x_p}{x_n} F\left(\frac{2x_n x_p}{x_n + x_p}\right) - \frac{1}{2} \frac{x_p}{x_n} F\left(\frac{2x_n x_p}{x_p - x_n}\right) + G(x_p) \\
F(x) &= 1 - \frac{3}{2} x \arctan \frac{1}{x} + \frac{1}{2} \frac{x^2}{1 + x^2} \\
G(x) &= 1 - x \arctan \frac{1}{x} \\
x_n &= m_{\pi^\pm} / 2p_{F,n} \simeq 0.207 (p_{F,n} / 1.68 \text{ fm}^{-1})^{-1} \\
x_p &= m_{\pi^\pm} / 2p_{F,p} \simeq 0.207 (p_{F,p} / 1.68 \text{ fm}^{-1})^{-1} \\
x_e &= m_{\pi^\pm} / 2p_{F,e} \simeq 0.207 (p_{F,e} / 1.68 \text{ fm}^{-1})^{-1}.
\end{aligned} \tag{S4}$$

- The dependence on the nucleon Fermi momenta,  $p_{F,n}$  and  $p_{F,p}$ , are identical to Refs. [35, 36]. Similarly the temperature dependence is identical. Both protons and neutrons are assumed to have the same temperature  $T$ .
- We add the factors of  $\beta_{nn} = 0.56$ ,  $\beta_{pp} = 0.7$ , and  $\beta_{np} = 0.66$ . These factors account for short-range correlations induced by the hard core of the nucleon-nucleon interactions. The nuclei interact by pion exchange, which corresponds to a Yukawa potential  $V(r)$ , but the potential is suppressed at separations smaller than the nucleon radius. In the context of neutrino emission, this effect was discussed in Refs. [88, 89], which also provide the numerical values that we use.
- We add the factors of  $\gamma_{nn} = \gamma_{pp} = \gamma_{np} = 0.838$ . The emissivities provided by Refs. [35, 36] are derived under the one-pion exchange approximation (OPE). Graphs with multiple pion exchanges can suppress the matrix element through a destructive interference. Following Ref. [40], we account for two-pion exchange with an effective one-meson exchange. Provided that the temperature is  $T < O(10 \text{ erg})$  and the momentum transfer is small compared to the pion mass, then the squared amplitude is suppressed by a momentum-independent factor of  $\gamma_{nn} \approx \gamma_{pp} \approx \gamma_{np} \approx (1 - C_\rho m_{\pi^0}^2 / m_\rho^2)^2 \simeq 0.838$  for  $C_\rho = 1.67$ ,  $m_{\pi^0} \simeq 134.976 \text{ erg}$  and  $m_\rho = 600 \text{ erg}$ .
- We account for a suppression of the nucleon couplings in high-density NS matter as compared to their values in vacuum. To see how this suppression arises, we first substitute  $f \rightarrow f^*$  and  $g_{aNN} \rightarrow g_{aNN}^*$  in the expressions from Refs. [35, 36] to indicate that these are in-medium couplings. Then

$$\left(\frac{f^*}{m_\pi}\right)^4 (g_{aNN}^*)^2 (m_N^*)^2 \approx \frac{g_{\pi NN}^4 g_{aNN}^2}{16m_N^2} \left(\frac{g_{\pi NN}^*}{g_{\pi NN}}\right)^4 \left(\frac{g_{aNN}^*}{g_{aNN}}\right)^2 \left(\frac{m_N^*}{m_N}\right)^{-2} \approx \frac{g_{\pi NN}^4 g_{aNN}^2}{16m_N^2} \gamma^6. \tag{S5}$$

In the first equality we have used  $f^*/m_\pi \approx g_{\pi NN}^*/2m_N^*$ . In the second equality we have used the scaling laws from [90]: the Goldberger-Treiman relation ( $g_{\pi NN}^*/g_{\pi NN} \approx (m_N^*/m_N)(g_A^*/g_A)(f_\pi^*/f_\pi)^{-1}$ ), the Brown-Rho scaling relation ( $m_N^*/m_N \approx (f_\pi^*/f_\pi)$ ), and the Mayle scaling relation ( $g_{aNN}^*/g_{aNN} \approx (m_N^*/m_N)(g_A^*/g_A)$ ). Then  $\gamma \approx (g_A^*/g_A)$  is given by [70]

$$\gamma = \left[1 + \frac{1}{3} \left(\frac{m_N^*}{m_N}\right) \left(\frac{p_{F,n}}{1.68 \text{ fm}^{-1}}\right)\right]^{-1}. \tag{S6}$$

Note that  $0 < \gamma < 1$ , such that  $\gamma \rightarrow 1$  for low-density NS matter, whereas for neutron densities a few times larger than the nuclear saturation density we have  $\gamma = O(0.1)$ . We neglect medium-dependent corrections to the pion mass, which could potentially enhance the axion emission rate [90]. The net effect of accounting for the medium-dependent couplings is to introduce a factor of  $(m_N^*/m_N)^{-2} \gamma^6$ .

- We add the factors of  $\mathcal{R}_{nn}$ ,  $\mathcal{R}_{pp}$ , and  $\mathcal{R}_{np}$  to account for a suppression of the bremsstrahlung rates due to superfluidity [89, 91]. When the NS core temperature falls below the superfluid critical temperature,  $T < T_c$ , nucleons can form Cooper pairs as the system partially condenses into a baryonic superfluid. As nucleons are bound into Cooper pairs, there are fewer free nucleons, which suppresses the bremsstrahlung rate exponentially.

If the temperature is not far below the critical temperature, Cooper pairs can also be broken by scattering. The formation and breaking of Cooper pairs can produce axions and neutrinos that carry away the liberated binding energy. If the NS matter is in the superfluid phase, these PBF processes provide the dominant axion production channels [92].

Phases of baryonic superfluids can be distinguished by the spin and flavor of the paired nucleons. In this work, we consider the spin-0  $S$ -wave neutron-neutron pairing, the spin-0  $S$ -wave proton-proton pairing, and the spin-1  $P$ -wave neutron-neutron pairing (SM only). We do not consider the neutron-proton  $D$ -wave pairing, which is easily disrupted by a small difference between the proton and neutron densities [93]. Each pairing has an associated energy gap in the quasiparticle spectrum, called the superfluid pairing gap  $\Delta$ . For the neutron  $P$ -wave superfluidity, there are two possible types of pairings, called  $P^A$ -wave and  $P^B$ -wave, which differ in the anisotropy of the gap energy [91, 92, 94]. We only include the  $P^A$ -wave pairing in our analysis, since the results are similar for the  $P^B$ -wave pairing. The temperature dependence of the pairing gaps are provided by [92], and the corresponding superfluid critical temperatures are provided by [95]. We do not account for uncertainties in the pairing gaps when deriving limits on the axion parameters. We find that our limits change by only a few percent between a model with no superfluidity and our fiducial model for  $S$ -wave superfluidity. Since this is small compared to other sources of uncertainty in our analysis, we do not expect an uncertainty in  $S$ -wave pairing gaps to have a significant impact on our results.

To determine whether neutron or protons form a superfluid at a given point within the star, we use the local densities to evaluate the corresponding superfluid critical temperatures [95]. For protons, if the local temperature is below the critical temperature for  $S$ -wave superfluidity, we say that a proton superfluid is present. For neutrons, we perform a similar comparison using the larger of the critical temperatures for the  $S$ -wave and  $P$ -wave pairings.

We evaluate the axion emissivity  $\varepsilon_a$  for each pairing. Expressions for the emissivities are provided by Refs. [46, 64, 69]. We modify these expressions to account for the medium-dependent couplings, which introduces a factor of  $(m_N^*/m_N)^2\gamma^2$ . Thus, the axion emissivities used in our work are

$$\begin{aligned} \text{PBF in } {}^1S_0(n) : \quad \varepsilon_a \simeq & (4.692 \times 10^{12} \text{ erg/cm}^3/\text{sec}) \left( \frac{g_{ann}}{10^{-10}} \right)^2 \left( \frac{p_{F,n}}{1.68 \text{ fm}^{-1}} \right)^3 \left( \frac{T}{10^8 \text{ K}} \right)^5 \\ & \times \left( \frac{m_n^*}{m_n} \right)^{-1} \left( \frac{\gamma}{1} \right)^2 \left( \frac{I_{a,n}^S}{0.022} \right) \end{aligned} \quad (\text{S7})$$

$$\begin{aligned} \text{PBF in } {}^1S_0(p) : \quad \varepsilon_a \simeq & (4.711 \times 10^{12} \text{ erg/cm}^3/\text{sec}) \left( \frac{g_{app}}{10^{-10}} \right)^2 \left( \frac{p_{F,p}}{1.68 \text{ fm}^{-1}} \right)^3 \left( \frac{T}{10^8 \text{ K}} \right)^5 \\ & \times \left( \frac{m_p^*}{m_p} \right)^{-1} \left( \frac{\gamma}{1} \right)^2 \left( \frac{I_{a,p}^S}{0.022} \right) \end{aligned} \quad (\text{S8})$$

$$\begin{aligned} \text{PBF in } {}^3P_2^A(n) : \quad \varepsilon_a \simeq & (3.769 \times 10^{13} \text{ erg/cm}^3/\text{sec}) \left( \frac{g_{ann}}{10^{-10}} \right)^2 \left( \frac{p_{F,n}}{1.68 \text{ fm}^{-1}} \right) \left( \frac{T}{10^8 \text{ K}} \right)^5 \\ & \times \left( \frac{m_n^*}{m_n} \right) \left( \frac{\gamma}{1} \right)^2 \left( \frac{I_{a,n}^{P^A}}{0.022} \right) \end{aligned} \quad (\text{S9})$$

$$\begin{aligned} \text{PBF in } {}^3P_2^B(n) : \quad \varepsilon_a \simeq & (3.769 \times 10^{13} \text{ erg/cm}^3/\text{sec}) \left( \frac{g_{ann}}{10^{-10}} \right)^2 \left( \frac{p_{F,n}}{1.68 \text{ fm}^{-1}} \right) \left( \frac{T}{10^8 \text{ K}} \right)^5 \\ & \times \left( \frac{m_n^*}{m_n} \right) \left( \frac{\gamma}{1} \right)^2 \left( \frac{I_{a,n}^{P^B}}{0.022} \right), \end{aligned} \quad (\text{S10})$$

where the temperature-dependent integrals  $I_{aN}^S$  are evaluated numerically and appear in Ref. [46]. If both neutrons and protons are in a superfluid phase, we sum the two emissivities. At low temperature,  $T \ll \Delta(T)$ , the emissivity is exponentially suppressed  $\propto e^{-2\Delta(T)/T}$ , since most nucleons settle into stable Cooper pairs, whereas axion emission requires the formation and breaking of pairs.

In the next subsection we present our similar modifications to the neutrino emissivities and discuss the quantitative effects of these corrections relative to previous works.

## B. Neutrino production rates

Neutrino emission from NS matter results from the direct URCA, modified URCA (MURCA) processes (both  $n$ -branch and  $p$ -branch), nucleon-nucleon bremsstrahlung, and PBF processes. The direct URCA processes correspond to the reactions  $n \rightarrow p + e + \bar{\nu}_e$  and  $p + e \rightarrow n + \nu_e$ . The MURCA processes in the  $N = n, p$  branch are  $n + N \rightarrow$

$N + p + e + \bar{\nu}_e$  and  $N + p + e \rightarrow n + N + \nu_e$ . (Note that we do not modify the direct URCA rates from those in NSCool because they are less relevant to this work, since the direct URCA process, which turns on at high NS masses, causes the NSs to cool too rapidly to explain the isolated NS luminosity data.) The corresponding emissivities are provided by Refs. [34, 88, 92, 96]. We reproduce these formulas here for completeness, and we update these formulas to account for the medium-dependent couplings in the same way that we did for the axion emissivities. This introduces a factor of  $\gamma^6(m_N^*/m_N)^{-4}$  for the MURCA and bremsstrahlung rates, and it introduces a factor of  $\gamma^2$  for the PBF rates; see (S6). We should emphasize that the same approximations were used to derive the neutrino emissivities as well as the axion emissivities above, and the nuclear physics factors are treated in the same way. The formulas are summarized by

$$\text{MURCA}(n): \quad \varepsilon_\nu \simeq (4.64 \times 10^{13} \text{ erg/cm}^3/\text{sec}) \left( \frac{p_{F,e}}{1.68 \text{ fm}^{-1}} + \frac{p_{F,\mu}}{1.68 \text{ fm}^{-1}} \right) \left( \frac{T}{10^8 \text{ K}} \right)^8 \quad (\text{S11})$$

$$\times \left( \frac{\alpha_n}{1} \right) \left( \frac{\beta_n}{0.68} \right) \left( \frac{\gamma_n}{0.838} \right) \left( \frac{\gamma}{1} \right)^6 \left( \frac{\mathcal{R}_n}{1} \right)$$

$$\text{MURCA}(p): \quad \varepsilon_\nu \simeq (4.62 \times 10^{13} \text{ erg/cm}^3/\text{sec}) \left( \frac{p_{F,e}}{1.68 \text{ fm}^{-1}} \right) \left( \frac{(p_{F,e} + 3p_{F,p} - p_{F,n})^2}{8p_{F,e}p_{F,p}} \right) \left( \frac{T}{10^8 \text{ K}} \right)^8 \quad (\text{S12})$$

$$\times \left( \frac{\alpha_p}{1} \right) \left( \frac{\beta_p}{0.68} \right) \left( \frac{\gamma_p}{0.838} \right) \left( \frac{\gamma}{1} \right)^6 \left( \frac{\mathcal{R}_p}{1} \right) \Theta(p_{F,e} + 3p_{F,p} - p_{F,n})$$

$$nn \rightarrow nn\nu\bar{\nu}: \quad \varepsilon_\nu \simeq (9.18 \times 10^{11} \text{ erg/cm}^3/\text{sec}) \left( \frac{p_{F,n}}{1.68 \text{ fm}^{-1}} \right) \left( \frac{T}{10^8 \text{ K}} \right)^8 \quad (\text{S13})$$

$$\times \left( \frac{\alpha_{nn}}{1} \right) \left( \frac{\beta_{nn}}{0.56} \right) \left( \frac{\gamma_{nn}}{0.838} \right) \left( \frac{\gamma}{1} \right)^6 \left( \frac{\mathcal{R}_{nn}}{1} \right)$$

$$np \rightarrow np\nu\bar{\nu}: \quad \varepsilon_\nu \simeq (2.16 \times 10^{12} \text{ erg/cm}^3/\text{sec}) \left( \frac{p_{F,p}}{1.68 \text{ fm}^{-1}} \right) \left( \frac{T}{10^8 \text{ K}} \right)^8 \quad (\text{S14})$$

$$\times \left( \frac{\alpha_{np}}{1} \right) \left( \frac{\beta_{np}}{0.66} \right) \left( \frac{\gamma_{np}}{0.838} \right) \left( \frac{\gamma}{1} \right)^6 \left( \frac{\mathcal{R}_{np}}{1} \right)$$

$$pp \rightarrow pp\nu\bar{\nu}: \quad \varepsilon_\nu \simeq (1.14 \times 10^{12} \text{ erg/cm}^3/\text{sec}) \left( \frac{p_{F,p}}{1.68 \text{ fm}^{-1}} \right) \left( \frac{T}{10^8 \text{ K}} \right)^8 \quad (\text{S15})$$

$$\times \left( \frac{\alpha_{pp}}{1} \right) \left( \frac{\beta_{pp}}{0.7} \right) \left( \frac{\gamma_{pp}}{0.838} \right) \left( \frac{\gamma}{1} \right)^6 \left( \frac{\mathcal{R}_{pp}}{1} \right)$$

$$\text{PBF in } ^1S_0(n): \quad \varepsilon_\nu \simeq (1.24 \times 10^{14} \text{ erg/cm}^3/\text{sec}) \left( \frac{m_n^*}{m_n} \right) \left( \frac{p_{F,n}}{1.68 \text{ fm}^{-1}} \right) \left( \frac{T}{10^8 \text{ K}} \right)^7 \left( \frac{\gamma}{1} \right)^2 \left( \frac{a_{n,s}}{1} \right) \left( \frac{F_A(v)}{1} \right) \quad (\text{S16})$$

$$\text{PBF in } ^1S_0(p): \quad \varepsilon_\nu \simeq (1.24 \times 10^{14} \text{ erg/cm}^3/\text{sec}) \left( \frac{m_p^*}{m_p} \right) \left( \frac{p_{F,p}}{1.68 \text{ fm}^{-1}} \right) \left( \frac{T}{10^8 \text{ K}} \right)^7 \left( \frac{\gamma}{1} \right)^2 \left( \frac{a_{p,s}}{1} \right) \left( \frac{F_A(v)}{1} \right) \quad (\text{S17})$$

$$\text{PBF in } ^3P_2^A(n): \quad \varepsilon_\nu \simeq (1.24 \times 10^{14} \text{ erg/cm}^3/\text{sec}) \left( \frac{m_n^*}{m_n} \right) \left( \frac{p_{F,n}}{1.68 \text{ fm}^{-1}} \right) \left( \frac{T}{10^8 \text{ K}} \right)^7 \left( \frac{\gamma}{1} \right)^2 \left( \frac{a_{n,t}}{1} \right) \left( \frac{F_B(v)}{1} \right) \quad (\text{S18})$$

$$\text{PBF in } ^3P_2^B(n): \quad \varepsilon_\nu \simeq (1.24 \times 10^{14} \text{ erg/cm}^3/\text{sec}) \left( \frac{m_n^*}{m_n} \right) \left( \frac{p_{F,n}}{1.68 \text{ fm}^{-1}} \right) \left( \frac{T}{10^8 \text{ K}} \right)^7 \left( \frac{\gamma}{1} \right)^2 \left( \frac{a_{n,t}}{1} \right) \left( \frac{F_C(v)}{1} \right), \quad (\text{S19})$$

where the  $\alpha$  factors are given by [88]

$$\alpha_n \approx \alpha_p \approx \frac{2}{(1 + 4x_n^2)^2} + \frac{2C}{1 + 4x_n^2} + 3C^2 \quad (\text{S20})$$

$$\alpha_{nn} \approx F(x_n) \quad (\text{S21})$$

$$\alpha_{np} \approx F(x_e) + \frac{2}{(1 + 4x_n^2)^2} + \frac{4C}{1 + 4x_n^2} + 6C^2 \quad (\text{S22})$$

$$\alpha_{pp} \approx F(x_p), \quad (\text{S23})$$

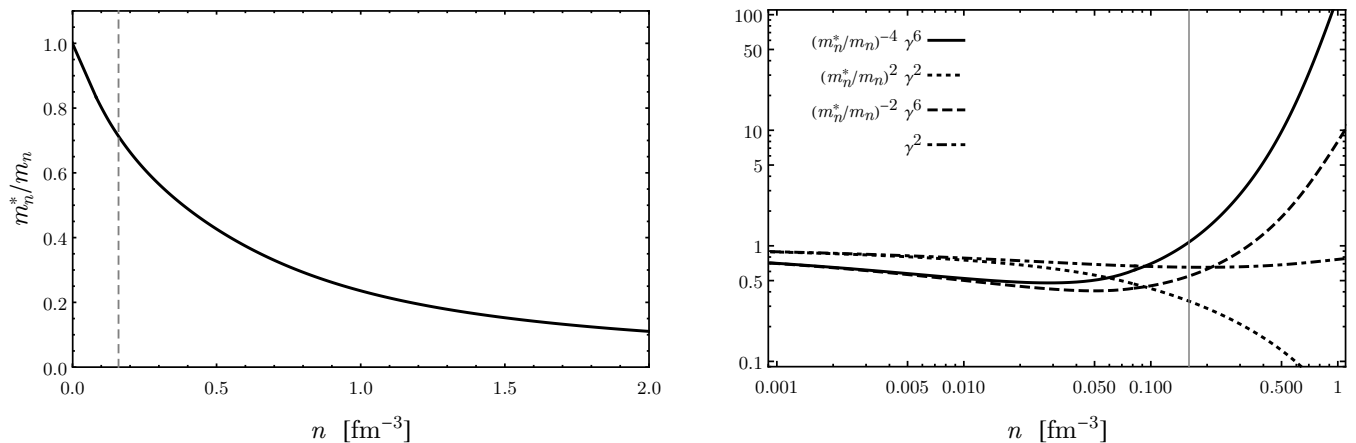


Figure S1. *Left:* The density-dependent neutron effective mass  $m_n^*$  compared to the vacuum mass  $m_n$  for the BSk22 EOS. *Right:* The density-dependent correction factors that are added to the axion and neutrino emissivity calculations to account for the medium-dependent effective couplings. At low density, all of these factors asymptote to 1.

with  $C \simeq -0.157$ . The  $a$  factors are given by [97]

$$a_{n,s} \approx g_A^2 v_{F,n}^2 \left[ (m_n^*/m_n)^2 + 11/42 \right] \quad (\text{S24})$$

$$a_{p,s} \approx g_A^2 v_{F,p}^2 \left[ (m_p^*/m_p)^2 + 11/42 \right] \quad (\text{S25})$$

$$a_{n,t} \approx 2g_A^2, \quad (\text{S26})$$

with  $g_A \simeq 1.26$  and  $v_{F,N} = p_{F,N}/m_N^*$ , and the  $F(v)$  factors are given by Ref. [92]. For the  $p$ -branch MURCA emissivity, we include momentum-dependent factor from Ref. [34], which corrects the factor from Ref. [96]. We set  $\beta_n = \beta_p = 0.68$ ,  $\beta_{nn} = 0.56$ ,  $\beta_{np} = 0.66$ ,  $\beta_{pp} = 0.7$ , and  $\gamma_n = \gamma_p = \gamma_{nn} = \gamma_{np} = \gamma_{pp} = 0.838$ .

For both the axion and neutrino emissivities, we introduced correction factors to account for the effective medium-dependent couplings. To assess the effect of these corrections, we plot these factors in Fig. S1 as a function of the neutron number density  $n$ . At the saturation density,  $n \simeq 0.16 \text{ fm}^{-3}$ , these factors are all close to 1 except for  $(m_n^*/m_n)^2 \gamma^2 \simeq 0.3$ , which suppresses the axion PBF emissivities. For typical stars in our cooling simulations, the maximal core density can be as large as  $n \approx 0.4 \text{ fm}^{-3}$ . At these higher densities,  $(m_n^*/m_n)^2 \gamma^2 \simeq 0.2$  suppresses the axion PBF emissivities, while  $(m_n^*/m_n)^{-4} \gamma^6 \simeq 5$  enhances the MURCA and neutrino bremsstrahlung rates. The factor  $\gamma^2 \approx 1$  across the whole range of NS densities, implying a negligible effect on the neutrino PBF emissivities. These corrections due to the effective medium-dependent couplings were not taken into account in previous studies of axion limits from NS cooling or SN 1987A. Thus, as mentioned in the main Letter, we estimate that the SN 1987A suggested upper limits in Ref. [40] should be a factor  $\sim 1.3$ – $1.6$  weaker, depending on the EOS, after the medium-dependent couplings have been accounted for. This is because that work computed the upper limits on axion couplings by requiring  $L_a^\infty/L_\nu^\infty < 1$ .

## II. STATISTICAL METHODOLOGY

Because our analysis includes a large number of nuisance parameters, many of which have degeneracies with each other and the signal parameter  $m_a$ , upper limits and possible detection significances cannot be interpreted in the asymptotic limit through Wilks' theorem. Instead, we determine limits and significances through MC procedures (see, e.g., [98]). We describe those procedures in detail in this section.

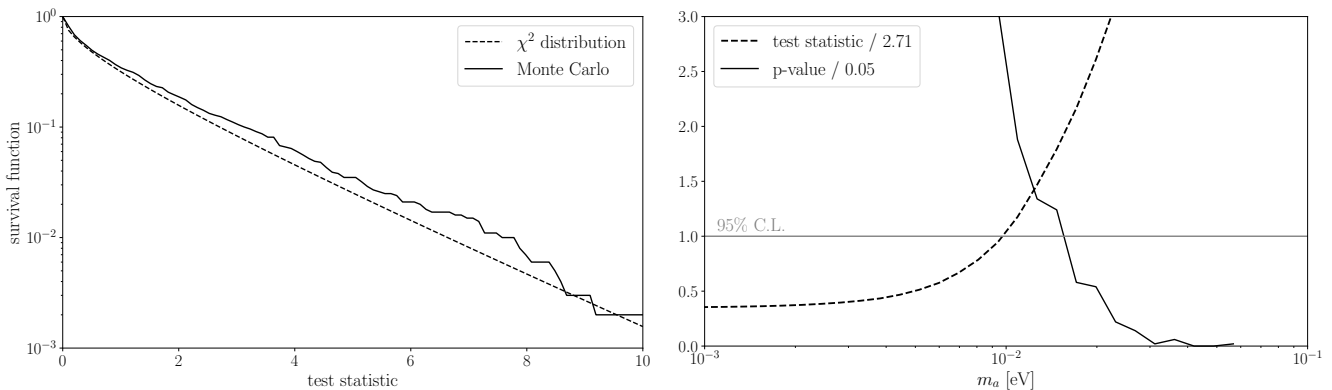


Figure S2. The MC distributions used to determine the detection significance of the axion model (left panel) and the 95% upper limit (right panel) for the KSVZ analysis that leads to the weakest 95% upper limit (BSk22 EOS and SFB-0-0 superfluidity model). We determine the detection significances and 95% upper limits through MC procedures by repeated simulations of the null and signal hypotheses. The detection significances are similar to those that would be obtained by assuming Wilks’ theorem but the upper limits tend to be more conservative by  $\sim 50\%$  when obtained by MC, as illustrated in the right panel. See text for details.

### A. Detection Significance

We use the test statistic  $q_0$  for the discovery of a signal in order to assess the significance of the axion hypothesis over the null hypothesis. This test statistic is defined as

$$q_0 = -2 \ln \frac{\mathcal{L}(\mathbf{d}|m_a = 0, \hat{\boldsymbol{\theta}}(0))}{\mathcal{L}(\mathbf{d}|\hat{m}_a, \hat{\boldsymbol{\theta}}(\hat{m}_a))}, \quad (\text{S27})$$

where  $\hat{m}_a$  is the axion mass at which  $\mathcal{L}(\mathbf{d})$  is globally maximized and  $\hat{\boldsymbol{\theta}}(m_a)$  is the nuisance parameter vector that maximizes  $\mathcal{L}(\mathbf{d})$  at fixed  $m_a$ . Recall that  $m_a < 0$  is allowed, with the axion emissivities multiplied by  $\text{sign}(m_a)$ . In order to assess for mismodeling we perform a two-sided significance test for the axion model, even though only positive axion masses are physical. A  $p$ -value for the improvement of the goodness-of-fit to the observed data with the inclusion of the axion signal parameter  $m_a$  can be obtained by

$$p = \int_{q_0, \text{obs}}^{\infty} f(q_0) dq_0, \quad (\text{S28})$$

where  $f(q_0)$  is the probability density function of the  $q_0$  under the null hypothesis. This  $p$ -value can then be associated with a significance (in terms of number of  $\sigma$ ) by  $\sqrt{\Phi^{-1}(1-p)}$ , where  $\Phi^{-1}$  is the inverse of the cumulative distribution function of the  $\chi^2$ -distribution. Since we are not in the asymptotic limit, rather than assuming  $f$  is the probability density function of the  $\chi^2$  distribution, we will determine it through the following MC procedure.

After fitting the null hypothesis to the observed data, we have  $\hat{\boldsymbol{\theta}}(0)$ , which contain a maximum-likelihood age under the null for each star  $\mathbf{t} = \{\hat{t}^i(0)\}$ . We also compute the set of maximum-likelihood luminosities  $\mathbf{L} = \{L(0, \hat{\boldsymbol{\theta}}^i(0))\}$  from  $\hat{\boldsymbol{\theta}}(0)$ . A single MC realization of the data under the null is then constructed by  $\mathbf{d}_{\text{MC}}^i = \{L^i + \delta L^i, \sigma_L^i, \mathbf{t}^i + \delta \mathbf{t}^i, \sigma_t^i\}$  where  $\delta L^i$  and  $\delta \mathbf{t}^i$  are variates drawn from a zero-mean Gaussian distribution with standard deviation  $\sigma_L^i$  and  $\sigma_t^i$ , respectively. These quantities represent the measured luminosity and measured age of the NS within the MC realization. Note that infrequently, we may have  $\mathbf{t}^i + \delta \mathbf{t}^i < 0$ , which we address by flooring the MC measured age at 0. For a given realization of the MC data, we compute

$$q_0^{\text{MC}} = -2 \ln \frac{\mathcal{L}(\mathbf{d}_{\text{MC}}|m_a = 0, \hat{\boldsymbol{\theta}}(0))}{\mathcal{L}(\mathbf{d}_{\text{MC}}|\hat{m}_a, \hat{\boldsymbol{\theta}}(\hat{m}_a))}, \quad (\text{S29})$$

from which we infer  $f(q_0)$  and determine a detection significance associated with  $q_0$  as calculated from the observed data. This procedure is performed independently for each combination of EOS and superfluidity model.

In the left panel of Fig. S2 we illustrate the survival function for the  $\chi^2$ -distribution (dashed) as a function of the discovery test statistic  $q_0$ . We compare this distribution to the distribution of  $p$ -values, as defined in (S28), over

an ensemble of  $10^3$  MC realizations. This is the discovery test statistic distribution for our EOS and superfluidity combinations that leads to the weakest upper limit for our KSVZ analysis (BSk22 EOS and SFB-0-0 superfluidity model). Note that in this case finite test statistics are somewhat less significant than they would be under the  $\chi^2$  distribution, though for other EOS and superfluidity combinations the opposite is true.

## B. Upper Limits

The procedure for setting a 95% upper limit follows a similar MC approach as that used to determine a detection significance. We now consider a test statistic  $q_{m_a}$  for upper limits defined by

$$q_{m_a} = \begin{cases} -2 \ln \frac{\mathcal{L}(\mathbf{d}|m_a, \hat{\theta}(m_a))}{\mathcal{L}(\mathbf{d}|\hat{m}_a, \hat{\theta}(\hat{m}_a))} & \hat{m}_a < m_a, \\ 0 & \hat{m}_a \geq m_a, \end{cases} \quad (\text{S30})$$

The compatibility between the data and a hypothesized value  $m_a$  for the axion mass is quantified by the  $p$ -value

$$p_{m_a} = \int_{q_{m_a}}^{\infty} f(q_{m_a}|m_a) dq_{m_a}, \quad (\text{S31})$$

where  $f(q_{m_a}|m_a)$  is the probability density function for the distribution of  $q_{m_a}$  under the assumption that the axion has mass  $m_a$ . The 95% upper limit on  $m_a$  is then determined at  $m_a^{95}$  where  $p_{m_a^{95}} = 0.05$ . As in the case of determining the distribution relevant for detection significance, we will use a MC procedure to determine probability density functions, though now we are determining through MC a family of distributions parametrized by the assumed value of  $m_a$ .

Specifically, for a range of values of  $m_a$ , we determine  $\hat{\theta}(m_a)$ , providing the maximum-likelihood estimate of the age under the assumed  $m_a$  and enabling us to calculate maximum-likelihood luminosities  $\mathbf{L}(m_a) = \{L(m_a, \hat{\theta}^i(0))\}$  from  $\hat{\theta}(m_a)$ . Similar to before, a single MC realization under the assumed  $m_a$  is constructed by  $\mathbf{d}_{\text{MC}}^i = \{\mathbf{L}^i + \delta L^i, \sigma_L^i, \mathbf{t}^i + \delta \mathbf{t}^i, \sigma_t^i\}$ . For each MC realization, we compute  $q_{m_a}^{\text{MC}}$  defined by

$$q_{m_a}^{\text{MC}} = \begin{cases} -2 \ln \frac{\mathcal{L}(\mathbf{d}_{\text{MC}}|m_a, \hat{\theta}(m_a))}{\mathcal{L}(\mathbf{d}_{\text{MC}}|\hat{m}_a, \hat{\theta}(\hat{m}_a))} & \hat{m}_a < m_a, \\ 0 & \hat{m}_a \geq m_a, \end{cases} \quad (\text{S32})$$

and then calculate  $p_{m_a}$  from the MC distribution. We then vary  $m_a$  until  $p_{m_a} = 0.05$  to determine our 95% upper limit. As before, this procedure is performed independently for each combination of EOS and superfluidity model.

In the right panel of Fig. S2 we illustrate the  $p_{m_a}$  that we determine through the MC procedure for the KSVZ analysis that leads to the weakest limit (BSk22 EOS and SBF-0-0 superfluidity model, as in the left panel). Note that the  $p$ -value distribution has been rescaled such that the one-sided 95% upper limit is achieved when the curve crosses unity. On the same figure we illustrate the test statistic itself, as defined in (S30). In the asymptotic limit where Wilks' theorem holds the 95% one-sided upper limit should be given by where the test statistic crosses  $\sim 2.71$  (see, *e.g.*, [98]), though again we have rescaled the test statistic such that the Wilks' limit is achieved for the curve crossing unity. Comparing the limit obtained through the MC procedure to that obtained by assuming Wilks' theorem we see that the MC limit is more conservative by  $\sim 50\%$  in  $m_a$ .

## III. EXTENDED RESULTS

In this section we present additional results related to the analyses discussed in the main Letter. The EOS that are consistent with the mass-radius relation (BSk22, BSk24, BSk25) determined by [76] and inconsistent (APR, BSk26) are illustrated in Fig. S3. Note that the green and gold bands show the containment regions determined from that work at the indicated confidence. Ref. [76] combined mass-radius measurements of PSR J0030 [75] and PSR J0740 [76], made with *NICER* data, with gravitational wave data from NS mergers in the context of a non-parametric mass-radius model based off of Gaussian Process modeling.

### A. Extended results for fiducial analyses

In Tab. S1 we present the full results from the analyses of the different EOS and superfluidity combinations for the KSVZ axion. We present the 95% upper limits ( $m_a^{95}$ ), the best-fit axion masses ( $\hat{m}_a$ ), allowing the best-fit masses

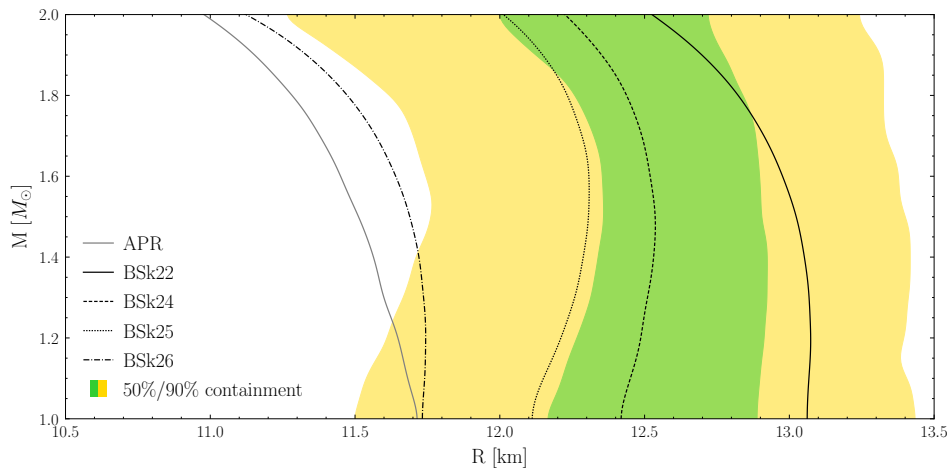


Figure S3. Green and gold bands show the containment regions (at indicated confidence) for the NS mass and radius as constructed in [76]. That work made use of simultaneous mass-radius measurements of two NSs, PSR J0030 [75] and PSR J0740 [76], with *NICER* data, in conjunction with gravitational wave data from NS mergers. On top of the containment regions we illustrate the mass-radius predictions from the five EOS considered in this work. The APR and BSk26 EOS are not consistent within 90% with the mass-radius data and are thus not considered in our fiducial analyses, though results with these EOS are presented in the SM.

to be negative with the axion luminosities multiplied by  $\text{sign}(m_a)$ , the significance of the axion model over the null hypothesis under the two-sided test, and the absolute  $\chi^2$  value of the null hypothesis test. The significance is quoted in terms of  $\sigma$  as determined by our MC procedure described in Sec. II A. The  $\chi^2$  value of the null hypothesis is defined by

$$\chi^2 \equiv \sum_i \frac{[L(0, \hat{\theta}^i) - L_0^i]^2}{(\sigma_L^i)^2} + \frac{(\hat{t}^i - t_0^i)^2}{(\sigma_t^i)^2}, \quad (\text{S33})$$

with the sum over the five NSs and the notation as in (2). Note that  $\hat{\theta}^i$  denotes the best-fit model parameter vector under the null hypothesis ( $m_a = 0$ ). Smaller values of  $\chi^2$  denote better fits of the null hypothesis, though keep in mind that many of the  $\chi^2$  values are smaller than unity because of the large number of nuisance parameters. Still, the  $\chi^2$  values clearly show that some superfluidity and EOS models provide worse fits to the data than others. The best-fitting model under the null hypothesis is the BSk22 EOS with no superfluidity. In Tabs. S2, S3, S4, S5, and S6, we show the best-fit nuisance parameters for the individual NSs under the null hypothesis for the different EOS and superfluidity combinations. Note that many of the NSs have best-fit masses near or at  $1M_\odot$ , which is the lower edge of our mass prior. However, as we show, the dependence of our results on the NS mass is relatively minor, so long as the mass is not large enough for the direct URCA process to be important.

In Fig. S4 we show the test statistic for upper limits, defined in (S30), for the individual NSs considered in this work as functions of the KSVZ axion mass  $m_a$ . Note that these curves extend to negative masses, though they are only illustrated for positive masses. We illustrate the test statistics assuming the SFB-0-0 superfluidity model and the BSk22 EOS, since that leads to the most conservative limits for the KSVZ axion. As described in Sec. II B, assuming Wilks' theorem is not a good approximation in determining the upper limit and leads to an overestimate of the limit by  $\sim 50\%$ . Still, for the purpose of comparing the relative importance of different NSs it is instructive to compare their upper-limit test statistics. Recall that assuming Wilks' theorem the 95% upper limits are determined by where these curves cross  $\sim 2.71$ . From Fig. S4 we see that the most constraining NS is J1605, followed by J0720 and J1308.

In the main Letter we interpreted our results in the context of the KSVZ and DFSZ QCD axion models. In Fig. S5 we take a more phenomenological approach and consider axion models characterized by coupling strengths  $g_{ann}$  and  $g_{app}$  to neutrons and protons, respectively. The shaded region in that parameter space is excluded by our analysis at 95% confidence. To construct this figure we fix the ratio  $g_{ann}/g_{app}$  and then construct the likelihood profile as a function of  $g_{ann}$ . The presented limits are then the one-sided 95% upper limits constructed from our MC procedure.

|           | Bsk22   | Bsk24  | Bsk25  | Bsk26  | APR   |
|-----------|---|--|--|--|---|
| 0-0-0     | $m_a^{95}=14$ meV<br>$\hat{m}_a=-8.1$ meV<br>$\sigma=0.36$<br>$\chi^2=0.46$ | $m_a^{95}=12$ meV<br>$\hat{m}_a=-9.4$ meV<br>$\sigma=0.8$<br>$\chi^2=0.99$ | $m_a^{95}=8.8$ meV<br>$\hat{m}_a=-9.4$ meV<br>$\sigma=1.1$<br>$\chi^2=1.8$ | $m_a^{95}=13$ meV<br>$\hat{m}_a=-11$ meV<br>$\sigma=0.83$<br>$\chi^2=1$  | $m_a^{95}=4.7$ meV<br>$\hat{m}_a=-11$ meV<br>$\sigma=1.4$<br>$\chi^2=3$   |
| SFB-0-0   | $m_a^{95}=16$ meV<br>$\hat{m}_a=-9.4$ meV<br>$\sigma=0.92$<br>$\chi^2=1.2$  | $m_a^{95}=13$ meV<br>$\hat{m}_a=-9.4$ meV<br>$\sigma=1.1$<br>$\chi^2=1.9$  | $m_a^{95}=9.3$ meV<br>$\hat{m}_a=-11$ meV<br>$\sigma=1.5$<br>$\chi^2=2.9$  | $m_a^{95}=14$ meV<br>$\hat{m}_a=-13$ meV<br>$\sigma=1.2$<br>$\chi^2=2$   | $m_a^{95}=3.4$ meV<br>$\hat{m}_a=-13$ meV<br>$\sigma=1.9$<br>$\chi^2=4.8$ |
| SFB-0-T73 | $m_a^{95}=15$ meV<br>$\hat{m}_a=-8.1$ meV<br>$\sigma=0.83$<br>$\chi^2=1.8$  | $m_a^{95}=10$ meV<br>$\hat{m}_a=-9.4$ meV<br>$\sigma=1.5$<br>$\chi^2=2.9$  | $m_a^{95}=6$ meV<br>$\hat{m}_a=-11$ meV<br>$\sigma=1.6$<br>$\chi^2=4.2$    | $m_a^{95}=10$ meV<br>$\hat{m}_a=-11$ meV<br>$\sigma=1.3$<br>$\chi^2=2.3$ | $m_a^{95}=4.6$ meV<br>$\hat{m}_a=-13$ meV<br>$\sigma=1.9$<br>$\chi^2=5.2$ |

Table S1. 95% C.L. limit  $m_a^{95}$ , best-fit axion mass  $\hat{m}_a$ , and significance  $\sigma$  of the best fit under the KSVZ axion model for different combinations of EOS and superfluidity model. We also provide the  $\chi^2$  quantity which describes the goodness-of-fit of the null model. Note that significance  $\sigma$  is computed through the MC procedure described in Sec. II A but is presented in the equivalent number of  $\sigma$  for a  $\chi^2$ -distributed discovery test statistic.

| <b>J1856</b> | Bsk22   | Bsk24   | Bsk25   | Bsk26   | APR   |
|--------------|---|---|---|---|---|
| 0-0-0        | $M_{\text{NS}} = 1.0M_{\odot}$<br>$\Delta M = 10^{-6}$  | $M_{\text{NS}} = 1.6M_{\odot}$<br>$\Delta M = 10^{-10}$ | $M_{\text{NS}} = 1.4M_{\odot}$<br>$\Delta M = 10^{-10}$ | $M_{\text{NS}} = 1.4M_{\odot}$<br>$\Delta M = 10^{-10}$ | $M_{\text{NS}} = 1.0M_{\odot}$<br>$\Delta M = 10^{-10}$ |
| SFB-0-0      | $M_{\text{NS}} = 1.0M_{\odot}$<br>$\Delta M = 10^{-8}$  | $M_{\text{NS}} = 1.4M_{\odot}$<br>$\Delta M = 10^{-10}$ | $M_{\text{NS}} = 1.0M_{\odot}$<br>$\Delta M = 10^{-10}$ | $M_{\text{NS}} = 1.2M_{\odot}$<br>$\Delta M = 10^{-10}$ | $M_{\text{NS}} = 1.8M_{\odot}$<br>$\Delta M = 10^{-12}$ |
| SFB-0-T73    | $M_{\text{NS}} = 1.0M_{\odot}$<br>$\Delta M = 10^{-10}$ | $M_{\text{NS}} = 1.8M_{\odot}$<br>$\Delta M = 10^{-12}$ |

Table S2. Best-fit nuisance parameters assuming no axion for the NS J1856 for different combinations of EOS and superfluidity model.

| <b>J1308</b> | Bsk22   | Bsk24   | Bsk25   | Bsk26   | APR   |
|--------------|---|---|---|---|---|
| 0-0-0        | $M_{\text{NS}} = 1.0M_{\odot}$<br>$\Delta M = 10^{-12}$ |
| SFB-0-0      | $M_{\text{NS}} = 1.0M_{\odot}$<br>$\Delta M = 10^{-12}$ | $M_{\text{NS}} = 1.2M_{\odot}$<br>$\Delta M = 10^{-12}$ | $M_{\text{NS}} = 1.2M_{\odot}$<br>$\Delta M = 10^{-12}$ | $M_{\text{NS}} = 1.0M_{\odot}$<br>$\Delta M = 10^{-12}$ | $M_{\text{NS}} = 1.6M_{\odot}$<br>$\Delta M = 10^{-14}$ |
| SFB-0-T73    | $M_{\text{NS}} = 1.0M_{\odot}$<br>$\Delta M = 10^{-12}$ | $M_{\text{NS}} = 1.6M_{\odot}$<br>$\Delta M = 10^{-14}$ |

Table S3. Best-fit nuisance parameters assuming no axion for the NS J1308 for different combinations of EOS and superfluidity model.

| <b>J0720</b> | Bsk22   | Bsk24   | Bsk25   | Bsk26   | APR   |
|--------------|---|---|---|---|---|
| 0-0-0        | $M_{\text{NS}} = 1.0M_{\odot}$<br>$\Delta M = 10^{-14}$ | $M_{\text{NS}} = 1.0M_{\odot}$<br>$\Delta M = 10^{-16}$ |
| SFB-0-0      | $M_{\text{NS}} = 1.0M_{\odot}$<br>$\Delta M = 10^{-14}$ | $M_{\text{NS}} = 1.2M_{\odot}$<br>$\Delta M = 10^{-16}$ |
| SFB-0-T73    | $M_{\text{NS}} = 1.0M_{\odot}$<br>$\Delta M = 10^{-14}$ | $M_{\text{NS}} = 1.2M_{\odot}$<br>$\Delta M = 10^{-16}$ | $M_{\text{NS}} = 1.0M_{\odot}$<br>$\Delta M = 10^{-18}$ | $M_{\text{NS}} = 1.0M_{\odot}$<br>$\Delta M = 10^{-16}$ | $M_{\text{NS}} = 1.4M_{\odot}$<br>$\Delta M = 10^{-20}$ |

Table S4. Best-fit nuisance parameters assuming no axion for the NS J0720 for different combinations of EOS and superfluidity model.

| <b>J1605</b> | Bsk22   | Bsk24   | Bsk25   | Bsk26   | APR   |
|--------------|---|---|---|---|---|
| 0-0-0        | $M_{\text{NS}} = 1.0M_{\odot}$<br>$\Delta M = 10^{-12}$ | $M_{\text{NS}} = 1.2M_{\odot}$<br>$\Delta M = 10^{-12}$ | $M_{\text{NS}} = 1.0M_{\odot}$<br>$\Delta M = 10^{-12}$ | $M_{\text{NS}} = 1.0M_{\odot}$<br>$\Delta M = 10^{-12}$ | $M_{\text{NS}} = 1.0M_{\odot}$<br>$\Delta M = 10^{-12}$ |
| SFB-0-0      | $M_{\text{NS}} = 1.0M_{\odot}$<br>$\Delta M = 10^{-12}$ | $M_{\text{NS}} = 1.2M_{\odot}$<br>$\Delta M = 10^{-12}$ | $M_{\text{NS}} = 1.2M_{\odot}$<br>$\Delta M = 10^{-12}$ | $M_{\text{NS}} = 1.0M_{\odot}$<br>$\Delta M = 10^{-12}$ | $M_{\text{NS}} = 1.4M_{\odot}$<br>$\Delta M = 10^{-14}$ |
| SFB-0-T73    | $M_{\text{NS}} = 1.0M_{\odot}$<br>$\Delta M = 10^{-12}$ | $M_{\text{NS}} = 1.4M_{\odot}$<br>$\Delta M = 10^{-14}$ |

Table S5. Best-fit nuisance parameters assuming no axion for the NS J1605 for different combinations of EOS and superfluidity model.

| <b>J0659</b> | Bsk22   | Bsk24   | Bsk25   | Bsk26   | APR   |
|--------------|---|---|---|---|---|
| 0-0-0        | $M_{\text{NS}} = 1.0M_{\odot}$<br>$\Delta M = 10^{-8}$  | $M_{\text{NS}} = 1.2M_{\odot}$<br>$\Delta M = 10^{-10}$ | $M_{\text{NS}} = 1.0M_{\odot}$<br>$\Delta M = 10^{-10}$ | $M_{\text{NS}} = 1.0M_{\odot}$<br>$\Delta M = 10^{-10}$ | $M_{\text{NS}} = 1.8M_{\odot}$<br>$\Delta M = 10^{-12}$ |
| SFB-0-0      | $M_{\text{NS}} = 1.0M_{\odot}$<br>$\Delta M = 10^{-10}$ | $M_{\text{NS}} = 1.0M_{\odot}$<br>$\Delta M = 10^{-10}$ | $M_{\text{NS}} = 1.0M_{\odot}$<br>$\Delta M = 10^{-20}$ | $M_{\text{NS}} = 2.0M_{\odot}$<br>$\Delta M = 10^{-20}$ | $M_{\text{NS}} = 1.6M_{\odot}$<br>$\Delta M = 10^{-12}$ |
| SFB-0-T73    | $M_{\text{NS}} = 1.0M_{\odot}$<br>$\Delta M = 10^{-10}$ | $M_{\text{NS}} = 1.0M_{\odot}$<br>$\Delta M = 10^{-10}$ | $M_{\text{NS}} = 1.6M_{\odot}$<br>$\Delta M = 10^{-12}$ | $M_{\text{NS}} = 1.8M_{\odot}$<br>$\Delta M = 10^{-12}$ | $M_{\text{NS}} = 1.6M_{\odot}$<br>$\Delta M = 10^{-12}$ |

Table S6. Best-fit nuisance parameters assuming no axion for the NS J0659 for different combinations of EOS and superfluidity model.

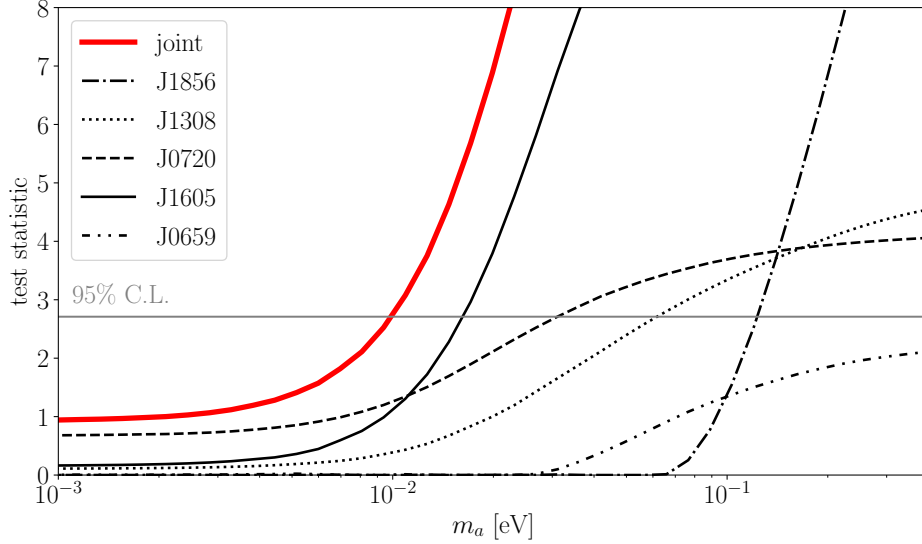


Figure S4. The test statistic for upper limits, defined in (S30) and in the context of the KSVZ axion model, for the individual NSs. These curves assume the SFB-0-0 superfluidity model and the BSk22 EOS. Assuming Wilks' theorem, the 95% upper limit is given by where the test statistic is equal to  $\sim 2.71$ , as indicated. The most constraining NS is J1605.

## B. Axions in younger neutron stars

In this work we focus on older NSs, with ages over  $\sim 10^5$  yrs. We find that younger NSs, including Cas A, are typically less constraining in the context of our modeling procedure, though a few younger NSs have comparable sensitivity. This point is illustrated in Fig. S6, where we compare the upper-limit test statistic (for the KSVZ axion) from the individual NSs considered in this work with those we determine from analyses of five younger NSs. Note that in Fig. S6 we show the EOS and superfluidity combinations that lead to the weakest limits, as estimated by the test statistic assuming Wilks' theorem, for the individual NSs. This is unlike in Fig. S4 where we show the individual test statistics for the EOS and superfluidity model that gives the weakest limit in the joint analysis over all five old, isolated NSs. The properties of the additional NSs are given in Tab. S7. For Cas A we also include the temperature derivative measurement from [50], who measure  $\dot{T}/T = (0.011 \pm 0.0046)/(10 \text{ yrs})$  assuming the Hydrogen column density was constant over all *Chandra* observations of Cas A. As mentioned in the main body, previous to [50] analyses of Cas A (such as [110, 111]) assumed strong superfluidity in order to explain the rapidly changing  $\dot{T}/T$ , but [50] pointed out that much of this cooling was instrumental in nature. Indeed, as shown in S6, the Cas A cooling data are consistent with the null hypothesis without  ${}^3P_2$  superfluidity, since the Cas A curve in Fig. S6 is for the model with no superfluidity and the BSk22 EOS. J173203 has also been the target of previous axion searches [112, 113] that found  $m_{a,\text{KSVZ}} < 0.085 \text{ eV}$  at 90% confidence. These works assumed that the age of J173203 was  $\sim 27 \text{ kyr}$  [114], which indeed would require a reduction in neutrino cooling rates to match the observed surface temperature, as discussed in [112, 113]. However, J173203 is actually a much younger NS, with an age  $4 \pm 2 \text{ kyr}$  [102–104], which is consistent with the standard cooling scenario and does not require unusual pairing gaps. We find that with the corrected NS data the constraint is relaxed. J172054 is a young NS which is naively interesting for axion searches given its well-measured luminosity of  $\sim (12 \pm 1) \times 10^{33} \text{ erg/s}$  [105]. However, this measurement assumes a fixed distance to Earth, and we find that after accounting for the distance measurement and uncertainty [51] J172054 is not a powerful probe. J0357,

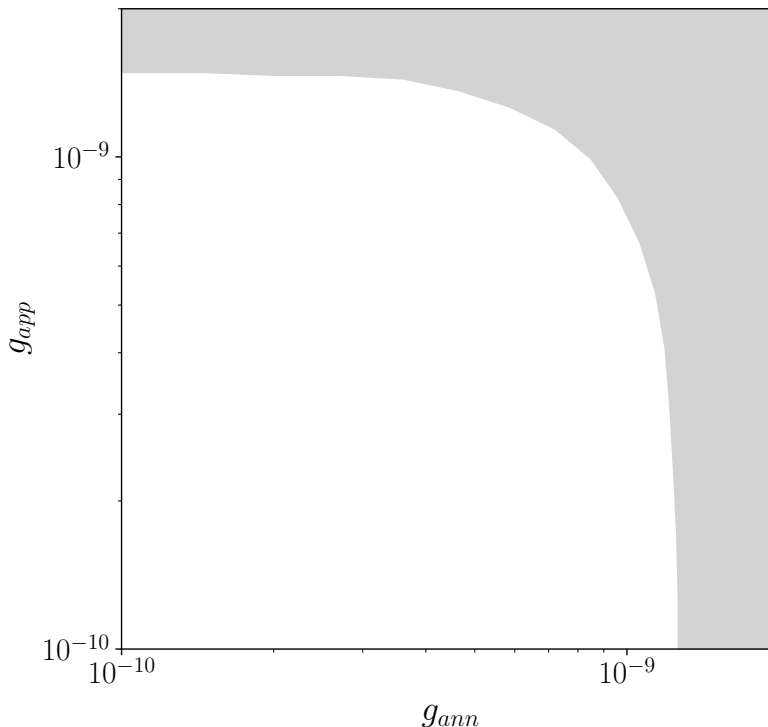


Figure S5. The one-sided 95% upper limits from this work in the plane of axion-neutron ( $g_{ann}$ ) and axion-proton ( $g_{app}$ ) couplings. The shaded region is excluded by our analysis; see text for details.

| Name    | $L_\gamma^\infty$ [ $10^{33}$ erg/s] | Age [yr]                     | Refs      |
|---------|--------------------------------------|------------------------------|-----------|
| Cas A   | —                                    | $330 \pm 19$                 | [99, 100] |
| J173203 | $17 \pm 10$                          | $(4 \pm 2) \times 10^3$      | [101–104] |
| J172054 | $11.4 \pm 4.4$                       | $650 \pm 50$                 | [105–107] |
| J0357   | $0.015 \pm 0.011$                    | $(7.5 \pm 5.5) \times 10^5$  | [108]     |
| J0538   | $1.09 \pm 0.47$                      | $(1.10 \pm 0.3) \times 10^5$ | [52, 109] |

Table S7. The properties of the supplemental NSs considered in this work: CXOU J232327.8+584842 (Cas A), XMMS J173203-344518 (J173203), XMMU J172054.5-372652 (J172054), PSR J0357+3205 (J0357), PSR J0538+2817 (J0538). Note that for Cas A we use measurements of its temperature  $T = (200.0 \pm 5) \times 10^4$  K (with the uncertainty roughly accounting for systematic differences in  $T$  measurements between different analyses, in addition to statistical uncertainties) and its temperature derivative  $\dot{T}/T = 0.0011 \pm 0.00046$  yr $^{-1}$  (with the value taken as that with fixed hydrogen column density, since it is the most conservative) rather than the luminosity measurement [50]. Also, to match the conventions of [50], the age of Cas A is presented at the reference epoch of 2011.49.

although older than  $10^5$  yr, has extremely uncertain luminosity and age measurements, so it is the least constraining NS in our analysis and we do not consider it in the main text. Finally, we include J0538 in the SM because its age is debated and could be a lower value than given in Tab. S7 of  $40 \pm 20$  kyr [109]. We find that in either case it is not constraining and so exclude it from our main analysis. As the ages and luminosities of some of the younger NSs become better understood in the future, it is likely that they will become more sensitive probes of axion-induced cooling.

### C. Effects of nuisance parameters

In Fig. S7 we illustrate the effects of the various nuisance parameters that we profile over in our analysis on NS cooling. We do not include axion in these simulations, and unless otherwise stated we fix the NS mass at  $M = 1.4M_\odot$ , the mass of light elements in the envelope  $\Delta M/M_\odot = 10^{-12}$ , the BSk24 EOS, and the SFB-0-0 superfluidity model. On top of the cooling curves which show the surface luminosity as a function of NS age, we indicate the data points

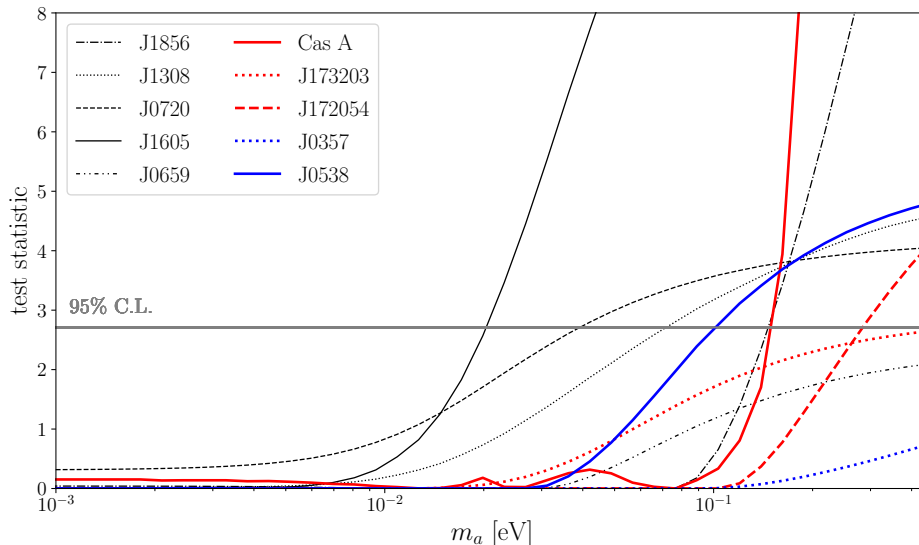


Figure S6. As in Fig. S4 but including the five younger NSs we consider in this work, whose properties are given in Tab. S7. Note that unlike in Fig. S4 here we display the test statistics for the EOS and superfluidity combinations that lead to the weakest limits for the individual NSs not the combination that leads to the weakest limit in a joint analysis.

for the isolated NSs that we consider in this work.

In the top-left panel we show the effect of varying  $\Delta M$ . Larger values of  $\Delta M$  increase the luminosity at early times but can rapidly decrease the luminosity at late times, for ages  $\sim 10^6$  yrs. The top-right panel indicates illustrates the varying NS mass. For this particular EOS masses larger than  $\sim 1.6 M_\odot$  reach high enough densities in the core to undergo direct URCA neutrino production and thus cool rapidly. The bottom-left panel varies the EOS. Apart from the BSk22 EOS, the the other EOSs give similar results. The BSk22 EOS is different in that already for  $M = 1.4 M_\odot$  the direct URCA process is allowed. Lastly, the bottom-right panel shows the effect of the superfluidity model. The  $^1S_0$  and no superfluidity models, which are our fiducial choices, produce similar results. The  $^3P_2$  pairing models that we consider in the SM. These models undergo rapid cooling at late times when the temperature drops below the  $^3P_2$  critical temperature, from PBF neutrino production, and are inconsistent with the M7 data. We discuss the  $^3P_2$  superfluidity models more in the next subsection.

#### D. $^3P_2$ superfluidity

In the right panel of Fig. S6 we showed that the  $^3P_2$  superfluidity models appear inconsistent with the isolated NS data. Here, we present further details of our  $^3P_2$  superfluidity tests. We consider four different superfluidity models, which are characterized by their zero-temperature gaps  $\Delta$  as functions of Fermi momenta. (Note that the critical temperatures are proportional to  $\Delta$ .) The first three models are denoted as models “a”, “b”, and “c” from [95], and, in NSCool, as SFB-a-T73, SFB-b-T73, and SFB-c-T73, respectively. (These NSCool models also self-consistently use the SFB  $^1S_0$  neutron gap model and the T73 proton  $^1S_0$  gap model.) However, more recent works indicate that the  $^3P_2$  gap may be substantially lower than in these models (see, *e.g.*, the recent review [79]). Of all the recent models reviewed in [79], the SCGF model with long and short range correlations from [115] has the lowest gap  $\Delta$  across all Fermi momenta. Thus, between the SCGF model and the models “a”, “b”, and “c” from [95], we span a large range of gaps discussed in the literature for the possible  $^3P_2$  pairing, though of course it is also possible that the gap is substantially lower such that  $^3P_2$  superfluidity never occurs (as we assume in the main Letter).

In the left panel of Fig. S8 we show the upper limit test statistics, for different EOS, as a functions of the KSVZ axion mass  $m_a$  for the indicated  $^3P_2$  gap models. Note that all of these models are inconsistent with the isolated NS data at more than  $\sim 3\sigma$ , as may be inferred from the test statistic at  $m_a = 0$  (more precisely, the axion model prefers a negative mass at more than  $3\sigma$ ). On the other hand, these models are much more sensitive to axions due to the PBF axion production mechanism. In the right panel of Fig. S8 we show how the neutrino PBF process leads to the rapid cooling for the  $^3P_2$  models, as seen in *e.g.* the right panel of Fig. S7. We illustrate the ratio of neutrino PBF luminosity ( $L_{\nu, \text{PBF}}^\infty$ ) to the bremsstrahlung neutrino luminosity plus  $L_\gamma^\infty$ . When this ratio is greater than unity it means that the PBF neutrino process dominates the cooling. Note that since the SCGF model has the lowest gap

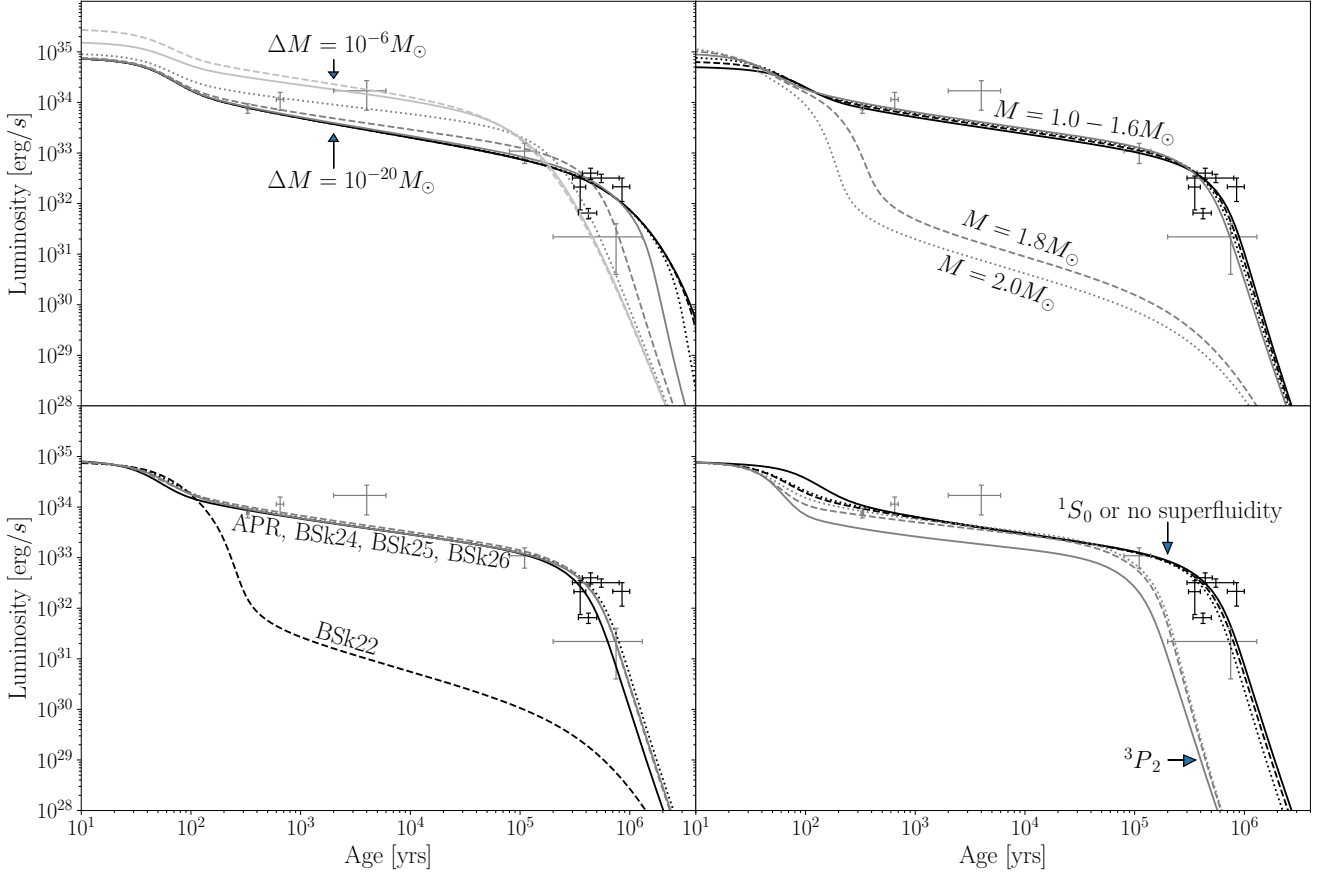


Figure S7. As in Fig. 1 except for an example NS with parameters, unless otherwise stated,  $M = 1.4 M_\odot$ ,  $\Delta M/M_\odot = 10^{-12}$ , the BSk24 EOS, and the SFB-0-0 superfluidity model. Each panel varies the indicated parameter, and no axions are included in the simulations. On top of the cooling curves we indicated the age and luminosity data for the isolated NSs considered in this work. The old NSs considered in our fiducial analysis are in black, while the data for the younger NSs that we analyze in the SM are in grey.

the  $^3P_2$  superfluidity turns on at the lowest temperature of the models considered. For this example we fix  $M = 1.4 M_\odot$  and  $\Delta M = 10^{-12} M_\odot$ .

We contrast the right panel of Fig. S8 with Fig. S9, where we illustrate similar luminosity ratios for the BSk22 EOS and a  $M = 1.0 M_\odot$  NS for the model with no  $^3P_2$  superfluidity but  $^1S_0$  neutron and proton superfluidity, as we consider in our fiducial analyses. (Note that the dependence on the EOS and NS mass is minor, and we also take  $\Delta M = 10^{-12} M_\odot$ .) For that figure we take the KSVZ axion model with  $m_a = 16$  meV, at our 95% upper limit. We show the ratios of the axion and neutrino PBF luminosities, for neutron and proton production, to the sum of the total neutrino and axion bremsstrahlung luminosities and the thermal surface luminosity. Comparing this figure with the right panel of Fig. S8 illustrates that the  $^3P_2$  pairing, if present, plays a much more important role on the NS thermal evolution than the  $^1S_0$  pairings.

### E. Sensitivity to the neutron star mass

In Fig. S7 we show that the NS cooling is not very sensitive to the NS mass unless the mass is large enough for the direct URCA process to become active. As an additional test of the effect of the NS mass on our final results, we consider including mass priors on J0720, J1308, and J1856. We do so following [116], who estimate that masses of these NSs as  $1.23^{+0.10}_{-0.05} M_\odot$  (J0720),  $1.08^{+0.20}_{-0.11} M_\odot$  (J1308), and  $1.24^{+0.29}_{-0.29} M_\odot$  (J1856) using gravitational redshift data. We analyze the cooling data for each of these NSs individually but we add to the likelihood an extra Gaussian contribution for the NS masses, centered on the mass estimates and with standard deviations given by the average of the upper and lower uncertainties from [116]. The results, shown in Fig. S10, indicate that the upper-limit test

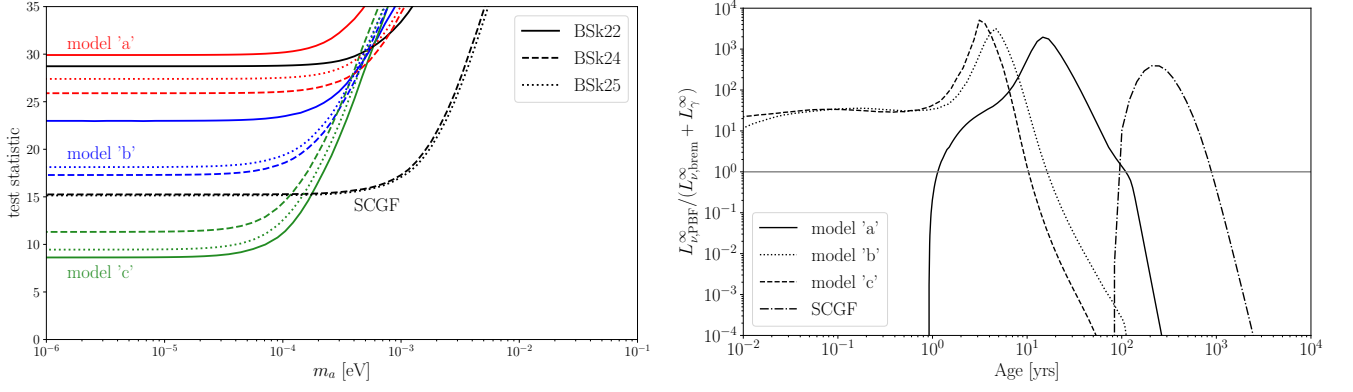


Figure S8.  ${}^3P_2$  superfluidity leads to rapid cooling of the NSs, as illustrated in the right panel of Fig. S7. (Left panel) We show the effects of including axions (for the KSVZ model) with  ${}^3P_2$  superfluidity, for the  ${}^3P_2$  gap models considered in this work. Note that the SCGF model has the lowest gap and model 'c' has the highest gap. The axion PBF process results in the NSs being much more sensitive to  $m_a$ , but on the other hand the  ${}^3P_2$  models appear inconsistent with the isolated NS data. (Right panel) Here, for the case  $m_a = 0$ , we show the neutrino PBF luminosity relative to the neutrino bremsstrahlung and thermal surface luminosities. When the neutrino PBF luminosity dominates the NS will undergo rapid cooling. Note that for this figure we fix  $M = 1.4 M_{\odot}$ .

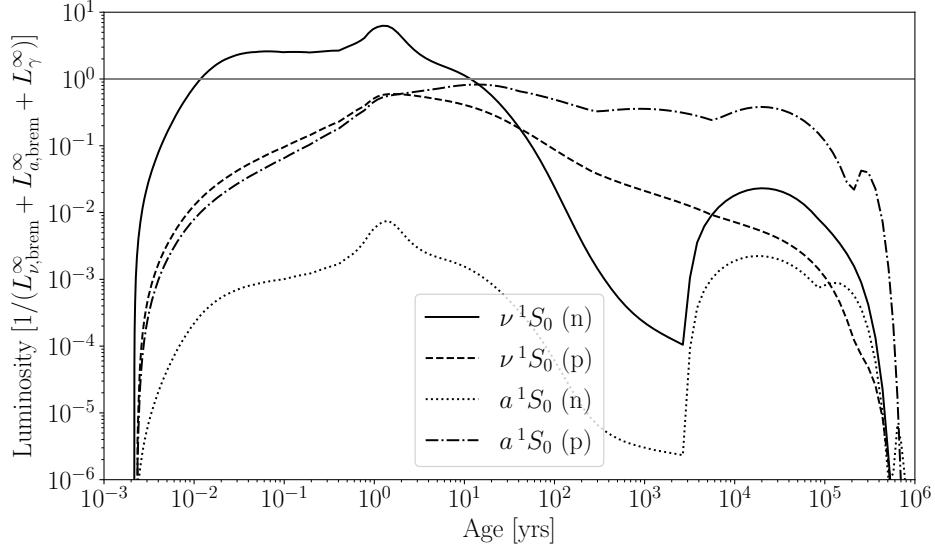


Figure S9. As in the right panel of Fig. S8 but for the BSk22 EOS, a  $1.0 M_{\odot}$  NS, and the superfluidity model with  ${}^1S_0$  neutron and proton pairings but no neutron  ${}^3P_2$  pairing. We additionally include a KSVZ QCD axion with  $m_a = 16$  meV. We show the ratios of the PBF luminosities for neutrinos and axions produced from neutrons and protons relative to the total bremsstrahlung luminosity plus the thermal surface luminosity. This figure illustrates that the PBF process plays a less important role for the  ${}^1S_0$  pairings than for the  ${}^3P_2$  pairing.

statistics are nearly identical with and without the inclusion of the mass priors.

#### IV. MAGNETIC FIELD DECAY

In this section consider the possible effects of magnetic field decay on the axion mass upper limits. We note that despite some dedicated efforts (*e.g.*, [117–128]) it is still not standard to include magnetic field decay in NS cooling, in part because the underlying mechanisms that transfer heat from the magnetic field to the NS matter are still not well understood. For example, while the magnetic field at the surface of a NS may be measured by *e.g.* spin-down – the M7 have field strengths  $\sim 10^{13}$  G – the magnetic fields within the NSs are not directly observable. The dissipation of

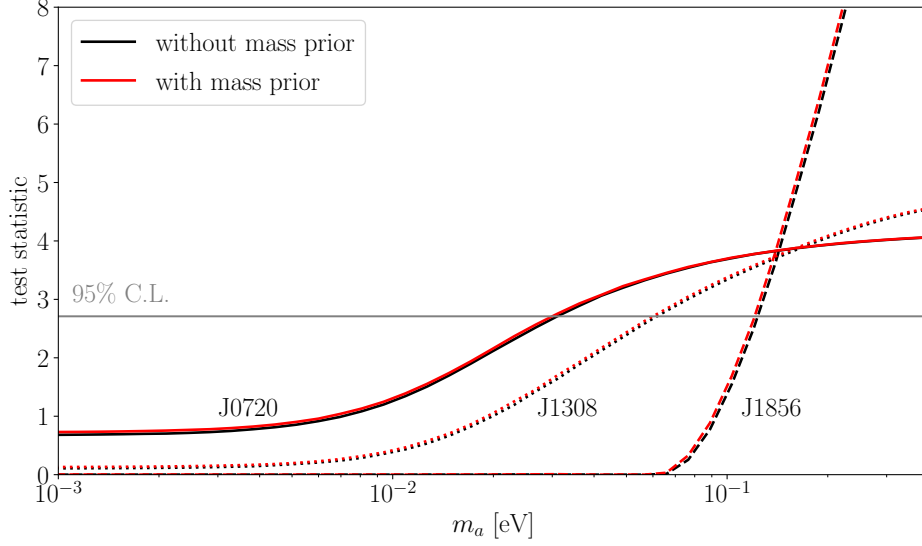


Figure S10. Mass estimates are available from [116] for the NSs J0720, J1308, and J1856. Here we consider including these mass estimates as priors in our analysis. As shown here, however, including the mass estimates makes little difference in our analysis.

energy from these fields into heat depends not only on the field strength and decay rate but also on the geometry of the fields within the NSs and the dissipative mechanisms, such as the electric conductivity, which are also uncertain. Still, there is evidence that old ( $\sim$ Myr-Gyr), isolated NSs, such as the M7, with stronger magnetic fields have higher surface temperatures than those with lower magnetic fields, suggesting that magnetic field decay may play a role in determining the surface temperature of isolated NSs in the epoch after neutrino emission dominates the energy loss, though this is far from conclusive (see, *e.g.*, [123]).

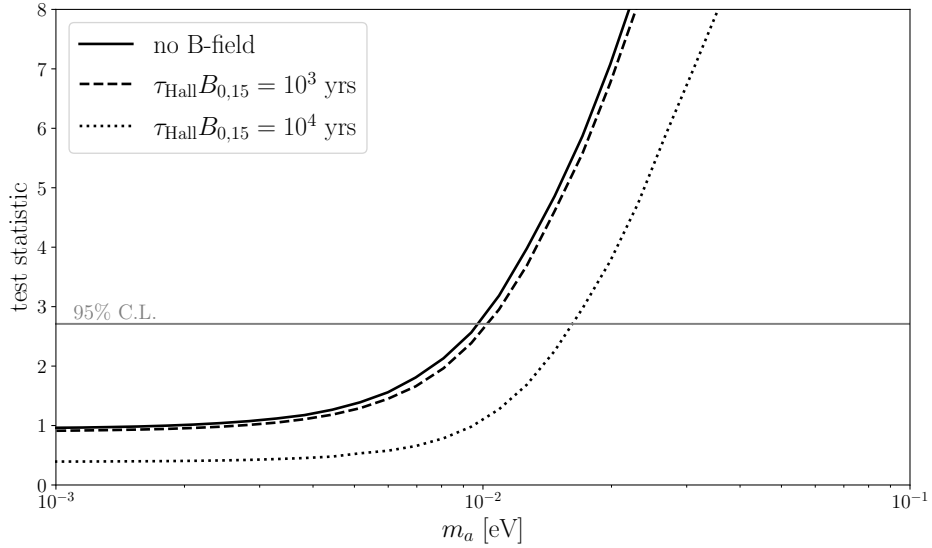


Figure S11. We test for the possible effects of magnetic field decay on our axion upper limits by using a parametric magnetic field decay model, where the magnetic field energy is dissipated in the crust as a heat source. The results depend sensitivity, in this model, on the Hall timescale. Using estimates (*e.g.*, [128]) that this timescale is less than  $\tau_{\text{Hall}} = 10^3 \text{ yr} / B_{0,15}$ , with  $B_{0,15}$  the value of the magnetic field in units of  $10^{15} \text{ G}$ , we conclude that B-field decay likely plays a subdominant role, as it produces similar results to the no B-field scenario. On the other hand, an increased Hall timescale, as illustrated, could weaken the upper limits. In these analyses we allow for initial magnetic fields up to  $10^{16} \text{ G}$  that fill the entire crust.

While complex 2D simulations of the coupled magneto-thermal evolution are now available (see [128] for the state-

of-the-art), we take a simpler approach in this work since, as we will show, the effect of magnetic field decay appears to be subdominant compared to other effects that we consider (though this should be checked with dedicated magnetothermal simulations incorporating axions). We follow instead the effective approach from *e.g.* [117, 123] and assume that the heat  $H$  from magnetic field decay (see (1) for the relation of  $H$  to  $L_\gamma^\infty$ ) is given simply by  $H = -V_{\text{eff}} B \dot{B}$ , where  $V_{\text{eff}}$  is the effective volume of the NS that supports the magnetic field  $B$ , with time derivative  $\dot{B}$ . As is standard, we assume that the dominant Joule heating arises from Ohmic dissipation in the crustal-confined magnetic fields, such that in our modified version of NSCool we only include energy injection from  $H$  into the crust. The magnetic energy is likely dissipated in hot-spots in the crust [123], such that  $V_{\text{eff}}$  is much smaller than the full volume of the crust. The double blackbody fits for the M7 indicate that the hot-spots have size of a few km across [57–61]. In these hot spots the magnetic field could be  $\sim 10$  times higher than the poloidal values [123]. To be conservative we assume  $V_{\text{eff}}$  is the full crustal volume, which is typically around 1/3 of the total NS volume, and we consider initial magnetic fields up to  $10^{16}$  G that fill the entire crust.

Following [125] we use the phenomenological parameterization of the magnetic field decay

$$B(t) = B_0 \frac{e^{-t/\tau_{\text{Ohm}}}}{1 + (\tau_{\text{Ohm}}/\tau_{\text{Hall}})(1 - e^{-t/\tau_{\text{Ohm}}})} \quad (\text{S34})$$

with  $B_0$  the initial magnetic field strength,  $\tau_{\text{Ohm}}$  the Ohmic dissipation timescale and  $\tau_{\text{Hall}}$  the Hall diffusion timescale. Ref. [125] suggests  $\tau_{\text{Ohm}} \sim 10^6$  yr and  $\tau_{\text{Hall}}$  up to  $\tau_{\text{Hall}} \sim 10^3$  yr/ $B_{0,15}$ , with  $B_{0,15} \equiv B_0/10^{15}$  G, though the Hall timescale could be faster. As a test we fix  $\tau_{\text{Ohm}} = 10^6$  yr (this timescale plays a less important role than the Hall timescale) and  $\tau_{\text{Hall}} = 10^3$  yr/ $B_{0,15}$ . In Fig. S11 we show the result of adding this heating contribution in the context of the KSVZ axion model upper limit test statistic profile. We compare the new result to that with no B-field decay, as considered in the main Letter. The difference between the two results is minimal. Smaller values of  $\tau_{\text{Hall}}$  lead to smaller differences, indicating that magnetic field decay likely plays a subdominant role. As a test, however, we consider increasing  $\tau_{\text{Hall}}$  by an order of magnitude to  $\tau_{\text{Hall}} = 10^4$  yr/ $B_{0,15}$ . In Fig. S11 we show that in this case the upper limit may be weakened by  $\sim 50\%$ . Given the potential relevance of magnetic field decay to the axion upper limits, this process should be investigated further in future works using more sophisticated treatments of the B-field decay.